

One-loop calculations of the decay of the next-to-lightest neutralino in the MSSM

MANUEL DREES^{1 *}, WOLFGANG HOLLIK^{2 †} AND QINGJUN XU^{2 ‡}

¹*Physikalisches Institut der Universität Bonn
Nussallee 12, D-53115 Bonn, Germany*

²*Max-Planck-Institut für Physik (Werner-Heisenberg-Institut)
Föhringer Ring 6, D-80805 Munich, Germany*

Abstract

We calculate one-loop corrections to the decays of the next-to-lightest neutralino $\tilde{\chi}_2^0$ into the lightest neutralino $\tilde{\chi}_1^0$ and two leptons; this includes diagrams where a real photon is emitted. In cases where two-body decays $\tilde{\chi}_2^0 \rightarrow \tilde{l}_1^\pm l^\mp \rightarrow \tilde{\chi}_1^0 l^- l^+$ are kinematically allowed, we calculate these decays both with and without the single-pole approximation, and find consistent results. For example, for the minimal supergravity parameter set SPS1a, the integrated partial widths (the branching ratios) for $\tilde{\chi}_2^0 \rightarrow \tilde{\chi}_1^0 l^- l^+$ ($l = e, \mu$) are enhanced by about 15.5 (13.6) percent by the one-loop corrections. We also study a scenario where $\tilde{\chi}_2^0$ cannot undergo two-body decays, and find corrections to these branching ratios of about 13.6 percent. Moreover, we study the dilepton invariant mass (M_{l+l^-}) distribution, whose endpoint is often used in analyses that aim to reconstruct (differences of) supersymmetric particle masses at the LHC. The shape of this distribution is altered significantly by the emission of hard photons. For example, for the SPS1a parameter set the peak of the M_{l+l^-} distribution is shifted by several GeV when these contributions are included.

*email: drees@th.physik.uni-bonn.de

†email: hollik@mppmu.mpg.de

‡email: qingjun.xu@physik.uni-freiburg.de

Present address: Physikalisches Institut, Albert-Ludwigs-Universität Freiburg
Hermann-Herder-Str. 3, D-79104 Freiburg, Germany

1 Introduction

Supersymmetry (SUSY) [1] is one of the best motivated extensions of the Standard Model (SM) of particle physics. If SUSY exists at the electroweak scale, experiments at future high energy colliders should be able to discover the superpartners of known particles, and to study their properties [2, 3]. From the precise measurement of the masses, production cross sections and decay branching ratios of these superpartners, the fundamental parameters of the underlying SUSY models can be determined. This will help us to reconstruct the SUSY breaking mechanism.

In the Minimal Supersymmetric Standard Model (MSSM) [1] with conserved R -parity, the lightest supersymmetric particle (LSP), which in many scenarios is the lightest neutralino $\tilde{\chi}_1^0$, appears at the end of the decay chain of each supersymmetric particle. The LSP escapes the detector, giving the characteristic SUSY signature of missing energy. While this helps to suppress backgrounds from SM processes, it also makes the measurement of supersymmetric particle masses more difficult. This is true in particular at hadron colliders like the LHC, where the total energy in a given partonic collision is not known.

At the LHC, the total SUSY production cross section is expected to be dominated by the production of gluinos and squarks, which decay into lighter charginos or neutralinos. Of particular interest are decay chains leading to the next-to-lightest neutralino $\tilde{\chi}_2^0$. $\tilde{\chi}_2^0$ in turn can always undergo the three-body decays $\tilde{\chi}_2^0 \rightarrow \tilde{\chi}_1^0 f \bar{f}$, at least for light SM fermions f . Depending on the neutralino, sfermion and Higgs boson masses, the two-body decays $\tilde{\chi}_2^0 \rightarrow \tilde{f} \bar{f} \rightarrow \tilde{\chi}_1^0 f \bar{f}$ and/or $\tilde{\chi}_2^0 \rightarrow \tilde{\chi}_1^0 Z/\phi \rightarrow \tilde{\chi}_1^0 f \bar{f}$ may also be open, where ϕ stands for one of the three neutral Higgs bosons of the MSSM; of course, Higgs intermediate states will contribute negligibly if $f = e$ or μ . These leptonic final states are of particular interest, since they can be identified relatively easily even at the LHC. Moreover, the dilepton invariant mass distribution can be measured accurately. In particular, the endpoint of this distribution is used in several analyses that aim to reconstruct (differences of) supersymmetric particle masses [2, 4]. Under favorable circumstances it has been shown that this endpoint can be measured to an accuracy of 0.1% at the LHC [2]. In order to match this accuracy, at least one-loop corrections to $\tilde{\chi}_2^0$ decays have to be included.

Turning to the planned e^+e^- linear collider ILC, $\tilde{\chi}_1^0 \tilde{\chi}_2^0$ production is often the first process that is kinematically accessible [5] (other than $\tilde{\chi}_1^0$ pair production, which leads to an invisible final state). The detailed analysis of $\tilde{\chi}_2^0$ decays can then yield information about heavier supersymmetric particles. Under favorable circumstances, $\mathcal{O}(10^4)$ $\chi_2^0 \rightarrow \chi_1^0 l^+ l^-$ decays may be observed at the ILC, again making the inclusion of quantum corrections mandatory to match the experimental precision. In this paper we present a complete calculation of these corrections in the MSSM.

The general MSSM has more than one hundred unknown free parameters. Therefore, it is not practicable to scan over the entire parameter space. Instead, several “benchmark scenarios” have been suggested [6], which are meant to illustrate characteristic features of various scenarios of SUSY breaking. Among those, the so-called SPS1a parameter set, which has been defined in the framework of the mSUGRA scenario [1], has been studied particularly widely. It gives rise to a particle spectrum where many states are accessible

both at the LHC and at a 500 GeV ILC [4]. The masses of the relevant neutralinos and sleptons at this benchmark point are listed in Table 1. Note in particular that the two-body decays $\tilde{\chi}_2^0 \rightarrow \tilde{l}_1^\pm l^\mp \rightarrow \tilde{\chi}_1^0 l^- l^+$ are kinematically allowed; here \tilde{l}_1 stands for the lighter one of the two charged sleptons of a given flavor. No other two-body decay mode is open. Moreover, squarks are so heavy that non-leptonic $\tilde{\chi}_2^0$ decays can be neglected in this scenario. Note that $\tilde{\chi}_1^0$ is mostly a $U(1)_Y$ gaugino (bino), while $\tilde{\chi}_2^0$ is dominated by its neutral $SU(2)$ gaugino (wino) component; this is typical for most scenarios where the gaugino mass unification relation holds [1]. Leptonic two-body decays of $\tilde{\chi}_2^0$ have been investigated at tree-level in Ref. [4], three-body decays of $\tilde{\chi}_2^0$ have been also studied at tree-level in Refs. [7, 8].

particle	$\tilde{\chi}_2^0$	$\tilde{\chi}_1^0$	$\tilde{e}_1 (\tilde{\mu}_1)$	$\tilde{e}_2 (\tilde{\mu}_2)$	$\tilde{\tau}_1$	$\tilde{\tau}_2$	$\tilde{\nu}_{e(\mu)}$	$\tilde{\nu}_\tau$
mass [GeV]	176.6	96.2	142.7	202.3	133.0	206.3	186.0	185.1

Table 1: Masses of the relevant neutralinos and sleptons for parameter set SPS1a [6].

In this paper, we calculate leptonic $\tilde{\chi}_2^0$ decays at one-loop level. Cases where $\tilde{\chi}_2^0$ has two-body decays $\tilde{\chi}_2^0 \rightarrow \tilde{l}_1^\pm l^\mp \rightarrow \tilde{\chi}_1^0 l^- l^+$ are treated both completely and in a single-pole approximation. In the complete calculation one has to employ complex slepton masses in the relevant propagators and one-loop integrals. The single-pole approximation in this case is performed by treating $\tilde{\chi}_2^0$ decays as the production and decay of the sleptons \tilde{l}_1 . We compare the results of both methods, and find good agreement for the SPS1a parameter set. We also analyze a scenario where $\tilde{\chi}_2^0$ only has three-body decays. In addition to calculating the integrated partial widths, we study the differential decay width of $\tilde{\chi}_2^0$ as a function of the dilepton invariant mass. If $\tilde{\chi}_2^0$ can undergo two-body decay, the shape of this distribution is essentially only affected by the emission of real photons; as well known, these contributions have to be added to the one-loop corrections to cancel infrared divergences. If $\tilde{\chi}_2^0$ only undergoes three-body decays, the shape of this distribution is also altered by the virtual corrections. In order to obtain the total decay width of $\tilde{\chi}_2^0$ and hence the branching ratios of its leptonic decays, the invisible decays $\tilde{\chi}_2^0 \rightarrow \tilde{\chi}_1^0 \nu_l \bar{\nu}_l$ and the hadronic decays $\tilde{\chi}_2^0 \rightarrow \tilde{\chi}_1^0 q \bar{q}$ are also calculated.

The paper is organized as follows. In Sec. 2 we briefly summarize the renormalization of those sectors of the MSSM which are relevant for the decays of $\tilde{\chi}_2^0$. The calculation of the tree-level decay widths is outlined in Sec. 3. Sec. 4 discusses how to calculate these decays at one-loop level, including the emission of real photons. The complete one-loop calculation and the one-loop calculation in the single-pole approximation are presented in Secs. 4.1 and 4.2, respectively. In Sec. 5 the total decay width of $\tilde{\chi}_2^0$ and the branching ratios of the leptonic decays are studied. Some numerical results are given in Sec. 6. We conclude our work in Sec. 7.

2 Renormalization of the MSSM

In order to calculate the higher-order corrections, one must renormalize the parameters and the fields of the MSSM. Several approaches for the renormalization of the MSSM have been developed [9, 10, 11, 12, 13, 14, 15]. Here we employ on-shell renormalization following the strategy of Refs. [12, 13]. This renormalization scheme is convenient for our purposes, since it ensures that the relevant supersymmetric particle masses are (almost) the same at one-loop level as at tree level; in particular, the endpoint of the $M_{\tilde{u}}$ distribution is the same in both cases. We assume here that all relevant parameters are real quantities; this amounts to the assumption that the soft-SUSY-breaking terms conserve CP.

2.1 Renormalization of the Chargino/Neutralino sector

Loop corrections to the masses and mixing angles of charginos and neutralinos were first discussed in Ref. [16]. The independent SUSY parameters in the chargino/neutralino mass matrices are the electroweak gaugino mass parameters M_1 , M_2 , and the supersymmetric Higgs mass parameter μ . These mass matrices also depend on the masses of the electroweak W and Z bosons, on the weak mixing angle θ_W , and on the ratio of vacuum expectation values (VEVs) $\tan\beta$; all these parameters are renormalized independently from the chargino/neutralino sector, as outlined below. In order to obtain finite S -matrix elements and Green's functions for chargino fields, we introduce a counterterm for the chargino mass matrix X , as well as field renormalization constants for the physical (mass eigenstate) four component (Dirac) chargino fields $\tilde{\chi}_i^{\pm}$ ($i = 1, 2$) [12]:

$$X \longrightarrow X + \delta X, \quad (1)$$

$$\begin{aligned} \omega_L \tilde{\chi}_i^+ &\longrightarrow \left(\delta_{ij} + \frac{1}{2} (\delta Z^L)_{ij} \right) \omega_L \tilde{\chi}_j^+, \\ \omega_R \tilde{\chi}_i^+ &\longrightarrow \left(\delta_{ij} + \frac{1}{2} (\delta Z^R)_{ij}^* \right) \omega_R \tilde{\chi}_j^+, \end{aligned} \quad (2)$$

where $\omega_{L,R} = (1 \mp \gamma_5)/2$. Each element of δX is the counterterm for the corresponding entry in X ; in particular, its diagonal entries are the counterterms δM_2 , $\delta \mu$. As for the fermionic fields of the SM, we need to introduce independent field renormalization constants for the left- and right-handed components of $\tilde{\chi}_i^{\pm}$. These constants δZ^L and δZ^R are general 2×2 matrices.

Similarly to the chargino case, we introduce renormalization constants for the neutralino mass matrix Y and for the physical four-component (Majorana) neutralino fields $\tilde{\chi}_i^0$ ($i = 1, 2, 3, 4$) [12]:

$$Y \longrightarrow Y + \delta Y, \quad (3)$$

$$\begin{aligned} \omega_L \tilde{\chi}_i^0 &= \left(\delta_{ij} + \frac{1}{2} (\delta Z^0)_{ij} \right) \omega_L \tilde{\chi}_j^0, \\ \omega_R \tilde{\chi}_i^0 &= \left(\delta_{ij} + \frac{1}{2} (\delta Z^0)_{ij}^* \right) \omega_R \tilde{\chi}_j^0. \end{aligned} \quad (4)$$

Here the elements of δY are the counterterms for the corresponding entries in Y ; in particular, the diagonal 2×2 blocks contain the counterterms δM_1 , δM_2 , and $\delta \mu$. The field renormalization constant δZ^0 is a general complex 4×4 matrix. Note that the Majorana condition $\tilde{\chi}_i^0 = (\tilde{\chi}_i^0)^C$ implies that the left- and right-handed components of $\tilde{\chi}_1^0$ do *not* renormalize independently, as shown in (4).

In the on-shell renormalization scheme for the charginos/neutralinos [12] the counterterms δM_2 , $\delta \mu$, and δM_1 are determined by requiring that the masses of $\tilde{\chi}_1^+$, $\tilde{\chi}_2^+$ and $\tilde{\chi}_1^0$, which are defined as the poles of the corresponding propagators, are the same as at tree-level. We have slightly modified this prescription, keeping $m_{\tilde{\chi}_1^0}$, $m_{\tilde{\chi}_2^0}$ and $m_{\tilde{\chi}_2^\pm}$ fixed, since $m_{\tilde{\chi}_2^0}$ is obviously more important for our analysis than $m_{\tilde{\chi}_1^\pm}$. The diagonal entries of the field renormalization constants are fixed by the condition that the corresponding renormalized propagator has unit residue. Furthermore, the renormalized one-particle irreducible two-point functions should be diagonal for on-shell external particles, which fixes the off-diagonal entries of the field renormalization constants. We note here that in this scheme the masses of the heavier neutralinos $\tilde{\chi}_{3,4}^0$ and lighter chargino $\tilde{\chi}_1^\pm$ do differ from their input (tree-level) values after one-loop corrections have been included. However, these shifts violate the electroweak $SU(2)$ symmetry, and are therefore usually quite small at least for gaugino-like states.¹ In most of mSUGRA parameter space (as well as in many other scenarios) the gaugino-like states are lighter than the higgsino-like ones. Moreover, gaugino-like states are usually produced more copiously in the decays of squarks and gluinos.

2.2 Renormalization of the Sfermion sector

In general the superpartners \tilde{f}_L , \tilde{f}_R of the fermions f_L , f_R mix to form the sfermion mass eigenstates \tilde{f}_s ($s = 1, 2$). The MSSM does not contain right-handed neutrino superfields, hence there is no $L - R$ mixing in the sneutrino sector. We assume that sfermions of different flavors do not mix. We renormalize the sfermion mass matrices $M_{\tilde{f}}$ and the sfermion fields \tilde{f}_s ($s = 1, 2$) via

$$M_{\tilde{f}} \longrightarrow M_{\tilde{f}} + \delta M_{\tilde{f}}, \quad (5)$$

$$\tilde{f}_s \longrightarrow \left(\delta_{st} + \frac{1}{2} (\delta Z_{\tilde{f}})_{st} \right) \tilde{f}_t. \quad (6)$$

The elements of the matrices $\delta M_{\tilde{f}}$ are the counterterms for the corresponding entries in $M_{\tilde{f}}$. The field renormalization constants $\delta Z_{\tilde{f}}$ are general 2×2 matrices. For the sneutrinos, their masses, their counterterms, and the field renormalization constants are simple numbers rather than matrices.

We follow Ref. [13] and renormalize the sfermion sector via the on-shell scheme. For every generation of the squarks, the independent parameters are the soft-breaking mass parameters $M_{\tilde{u}_L}^2 = M_{\tilde{d}_L}^2 \equiv M_{\tilde{q}_L}^2$, $M_{\tilde{u}_R}^2$, $M_{\tilde{d}_R}^2$ and the scalar trilinear coupling parameters A_u ,

¹In the presence of strong $L - R$ mixing in the stop sector, the masses of the higgsino-like neutralinos can still be shifted by several GeV [12, 17].

A_d . In order to fix their counterterms, one can renormalize two up-squarks and the lighter down-type squark via the on-shell renormalization scheme. It requires that the renormalized masses of the two up-type squarks and the lighter down-type squark are equal to their physical (input) masses, and that the renormalized two-point function is diagonal for on-shell external particles. These on-shell conditions determine the counterterms $\delta M_{\tilde{q}_L}^2$, $\delta M_{\tilde{u}_R}^2$, $\delta M_{\tilde{d}_R}^2$ as well as δA_u , δA_d and the off-diagonal entries of the field renormalization constant, under the assumption $\delta Z_{\tilde{q}_{12}} = \delta Z_{\tilde{q}_{21}}$. The independent parameters for the sleptons are $M_{\tilde{l}_L}^2$, $M_{\tilde{l}_R}^2$ and A_l . In analogy to the squarks, Ref. [13] renormalized the sleptons via imposing the on-shell renormalization conditions on the sneutrino and the lighter charged slepton. In a slight deviation from Ref. [13] we fix both charged slepton masses at their tree-level values. In general there will therefore be a shift of the mass of the sneutrino when one-loop corrections are included. However, since this shift again vanishes in the limit of exact electroweak gauge symmetry it is numerically very small [13, 18]. Similarly to the chargino/neutralino case, the diagonal entries of $\delta Z_{\tilde{f}}$ and the sneutrino field renormalization constant $\delta Z_{\tilde{\nu}_l}$ are fixed by the requirement that the corresponding propagator has unit residue. Besides the soft-breaking sfermion mass parameters and the scalar trilinear coupling parameters, the sfermion mass matrices $M_{\tilde{f}}$ also depend on μ , whose renormalization was discussed above, as well as on $\tan\beta$, m_Z , θ_W , the electric charge e and the charged fermion masses m_f , whose renormalization will be discussed below.

2.3 Renormalization of the neutral Higgs sector

The renormalization of the Higgs sector in the CP-violating MSSM has been described in Ref. [14]; here we limit ourselves to the neutral Higgs sector of the CP-conserving MSSM, using a mixture of on-shell and \overline{DR} renormalization.

The independent parameters in the Higgs sector are chosen to be the tadpoles T_{h^0} , T_{H^0} of the physical CP-even scalars h^0 and H^0 , which vanish at tree-level, the mass of the physical neutral CP-odd Higgs boson m_A^2 , and the ratio of VEVs $\tan\beta$ introduced above. In addition the counterterms from the renormalization of the weak gauge boson sector, described below, enter here.

In the neutral CP-odd Higgs boson sector, the mass matrix M_{χ^0} and the fields A^0 , G^0 are renormalized via

$$M_{\chi^0} \rightarrow M_{\chi^0} + \delta M_{\chi^0}, \quad (7)$$

$$\begin{pmatrix} A^0 \\ G^0 \end{pmatrix} \rightarrow \begin{pmatrix} 1 + \frac{1}{2}\delta Z_{AA} & \frac{1}{2}\delta Z_{AG} \\ \frac{1}{2}\delta Z_{GA} & 1 + \frac{1}{2}\delta Z_{GG} \end{pmatrix} \begin{pmatrix} A^0 \\ G^0 \end{pmatrix}. \quad (8)$$

Similarly, the neutral CP-even Higgs boson sector is renormalized as follows:

$$M_{\phi^0} \rightarrow M_{\phi^0} + \delta M_{\phi^0}, \quad (9)$$

$$\begin{pmatrix} h^0 \\ H^0 \end{pmatrix} \rightarrow \begin{pmatrix} 1 + \frac{1}{2}\delta Z_{hh} & \frac{1}{2}\delta Z_{hH} \\ \frac{1}{2}\delta Z_{Hh} & 1 + \frac{1}{2}\delta Z_{HH} \end{pmatrix} \begin{pmatrix} h^0 \\ H^0 \end{pmatrix}, \quad (10)$$

M_{ϕ^0} is the mass matrix of the CP-even Higgs bosons and the matrices δM_{χ^0} , δM_{ϕ^0} contain the counterterms δT_{h^0} , δT_{H^0} , δm_A^2 , and $\delta \tan \beta$.

The tadpole counterterms are fixed by the requirement that the renormalized tadpoles vanish. The counterterm δm_A^2 is determined by on-shell renormalization of the neutral CP-odd Higgs boson A^0 . In this paper, we fix the field renormalization constants in the Higgs sector as well as $\delta \tan \beta$ in the \overline{DR} scheme, which means that the counterterms only contain UV-divergent parts (plus some process-independent numerical constants).² In case of $\tan \beta$, this implies

$$\frac{\delta \tan \beta}{\tan \beta} = \frac{1}{2m_Z \sin \beta \cos \beta} [\text{Im} \Sigma_{A^0 Z}(m_A^2)]^{div}. \quad (11)$$

Other ways to renormalize $\tan \beta$ are discussed in Refs. [15, 19, 20].

2.4 Renormalization of the SM-like sector

The final piece of the Lagrangian we have to renormalize contains terms also present in the SM. Here we follow Ref. [21]. The relevant parameters are the electric charge e , the charged fermion masses m_f , and the masses of the W, Z bosons. They are renormalized as follows:

$$e \rightarrow (1 + \delta Z_e) e, \quad (12)$$

$$m_f \rightarrow m_f + \delta m_f, \quad (13)$$

$$m_{W,Z}^2 \rightarrow m_{W,Z}^2 + \delta m_{W,Z}^2. \quad (14)$$

The wave function renormalization of the fermion and neutral vector boson fields is described by

$$f_i^L \rightarrow \left(\delta_{ij} + \frac{1}{2} \delta Z_{ij}^{f,L} \right) f_j^L, \quad (15)$$

$$f_i^R \rightarrow \left(\delta_{ij} + \frac{1}{2} \delta Z_{ij}^{f,R} \right) f_j^R, \quad (16)$$

$$\begin{pmatrix} Z \\ A \end{pmatrix} \rightarrow \begin{pmatrix} 1 + \frac{1}{2} \delta Z_{ZZ} & \frac{1}{2} \delta Z_{ZA} \\ \frac{1}{2} \delta Z_{AZ} & 1 + \frac{1}{2} \delta Z_{AA} \end{pmatrix} \begin{pmatrix} Z \\ A \end{pmatrix}. \quad (17)$$

The renormalization constants above are again fixed by the on-shell conditions [21]. The on-shell definition of the weak mixing angle θ_W ($s_W = \sin \theta_W$, $c_W = \cos \theta_W$) is [22]

$$s_W^2 = 1 - \frac{m_W^2}{m_Z^2}. \quad (18)$$

²In the numerical examples discussed below, Higgs exchange contributions are negligible. However, they will be significant if $\tilde{\chi}_2^0 \rightarrow h^0 \tilde{\chi}_1^0$ decays are open, and/or at high $\tan \beta$, where the Yukawa couplings to charged leptons and charge 1/3 quarks are enhanced.

Hence its counterterm is directly related to the counterterms of the gauge boson masses,

$$\frac{\delta s_W}{s_W} = -\frac{1}{2} \frac{c_W^2}{s_W^2} \left(\frac{\delta m_W^2}{m_W^2} - \frac{\delta m_Z^2}{m_Z^2} \right). \quad (19)$$

This completes our discussion of the renormalization conditions. We are now ready to discuss the calculation of the $\tilde{\chi}_2^0$ decay width.

3 Tree-level calculations for $\tilde{\chi}_2^0 \rightarrow \tilde{\chi}_1^0 l^- l^+$

The Born Feynman diagrams for $\tilde{\chi}_2^0 \rightarrow \tilde{\chi}_1^0 l^- l^+$ ($l = e, \mu, \tau$) are displayed in Fig. 1. The propagators of the diagrams (a) and (b) have the structure as

$$\frac{1}{k^2 - m_{\tilde{l}_s}^2}, \quad (20)$$

where k and $m_{\tilde{l}_s}$ denote the 4-momentum of the propagator and the slepton mass, respectively. If the two-body decays $\tilde{\chi}_2^0 \rightarrow \tilde{l}_1^\pm l^\mp \rightarrow \tilde{\chi}_1^0 l^- l^+$ are kinematically allowed, i.e. the sleptons \tilde{l}_1 can be on shell at some points in the phase space, a finite width of \tilde{l}_1 is necessary. It arises from the imaginary part of the slepton self-energy. A finite width is introduced via Dyson summation,

$$\frac{i}{k^2 - m_{\tilde{l}_1}^2} + \frac{i}{k^2 - m_{\tilde{l}_1}^2} i\hat{\Sigma}(k^2) \frac{i}{k^2 - m_{\tilde{l}_1}^2} + \dots = \frac{i}{k^2 - m_{\tilde{l}_1}^2 + \hat{\Sigma}(k^2)}, \quad (21)$$

where $\hat{\Sigma}(k^2)$ is the renormalized \tilde{l}_1 self-energy.

A gauge invariant matrix element is obtained by a Laurent expansion around the complex pole [23]; in on-shell renormalization

$$\frac{1}{k^2 - m_{\tilde{l}_1}^2 + \hat{\Sigma}(k^2)} \simeq \frac{1}{k^2 - m_p^2} \left(1 - \frac{\text{Re}\hat{\Sigma}(k^2)}{k^2 - m_p^2} \right), \quad (22)$$

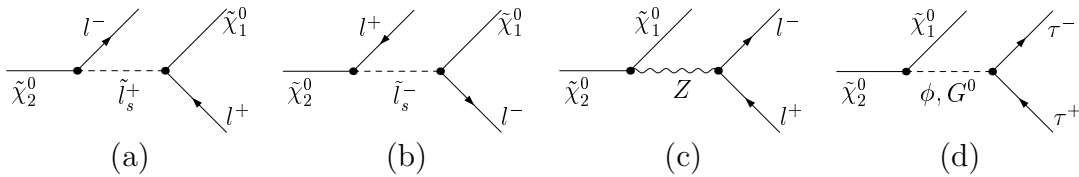


Figure 1: The Born Feynman diagrams for $\tilde{\chi}_2^0 \rightarrow \tilde{\chi}_1^0 l^- l^+$ ($l = e, \mu, \tau$). $s = 1, 2$ labels the slepton mass eigenstates, ϕ denotes the MSSM neutral Higgs boson h^0, H^0, A^0 , and the neutral Goldstone boson G^0 which appears only together with the Z boson in using a non-unitary gauge. Since the Yukawa coupling $\phi l^- l^+$ is proportional to the lepton mass, the Higgs intermediate states are neglected when $l = e$ and μ .

were m_p^2 denotes the position of the complex pole in (21). It is obtained as the solution of

$$m_p^2 - m_{\tilde{l}_1}^2 + \hat{\Sigma}(m_p^2) = 0. \quad (23)$$

For the tree-level amplitude the complex pole m_p^2 is calculated at one-loop level. Its explicit expression is

$$m_p^2 = m_{\tilde{l}_1}^2 - im_{\tilde{l}_1} \Gamma_{\tilde{l}_1}^{\text{tree}}, \quad (24)$$

where we have employed on-shell renormalization as in Sec. 2.2. $\Gamma_{\tilde{l}_1}^{\text{tree}}$ is the tree-level decay width of \tilde{l}_1 and $m_{\tilde{l}_1} \Gamma_{\tilde{l}_1}^{\text{tree}}$ is the imaginary part of the slepton self-energy $\Sigma(m_{\tilde{l}_1}^2)$. The first factor in (22) is nothing but the Breit-Wigner propagator. Since the second term in the parentheses in (22) is at one-loop level, we do not need it in the tree-level calculation. Therefore, the gauge invariant tree-level amplitude M_{tree} for the decays $\tilde{\chi}_2^0 \rightarrow \tilde{\chi}_1^0 l^- l^+$ can be written as

$$M_{\text{tree}} = \frac{V_{\tilde{\chi}_2^0 \tilde{l}_1^\pm l^\mp}^{\text{tree}}(k^2) V_{\tilde{l}_1^\pm \tilde{\chi}_1^0 l^\pm}^{\text{tree}}(k^2)}{k^2 - m_{\tilde{l}_1}^2 + im_{\tilde{l}_1} \Gamma_{\tilde{l}_1}^{\text{tree}}} + B(k^2), \quad (25)$$

where $V_{\tilde{\chi}_2^0 \tilde{l}_1^\pm l^\mp}^{\text{tree}}$ and $V_{\tilde{l}_1^\pm \tilde{\chi}_1^0 l^\pm}^{\text{tree}}$ represent the $\tilde{\chi}_2^0 \tilde{l}_1^\pm l^\mp$ and $\tilde{l}_1^\pm \tilde{\chi}_1^0 l^\pm$ vertices, respectively, and $B(k^2)$ denotes the non-resonant part of the matrix element, i.e. the matrix element of diagrams (a) and (b) for $s = 2$ and diagrams (c) and (d) in Fig. 1.

The non-resonant part is much smaller than the resonant one (diagrams (a) and (b) for $s = 1$ in Fig. 1), hence it can be neglected approximately. We can then compute the relevant partial widths in the single-pole approximation, where the decays $\tilde{\chi}_2^0 \rightarrow \tilde{\chi}_1^0 l^- l^+$ are treated as the production and decay of the sleptons \tilde{l}_1 ,

$$\Gamma(\tilde{\chi}_2^0 \rightarrow \tilde{\chi}_1^0 l^- l^+)_{\text{tree}} \simeq \Gamma(\tilde{\chi}_2^0 \rightarrow \tilde{l}_1^\pm l^\mp)_{\text{tree}} Br(\tilde{l}_1^\pm \rightarrow \tilde{\chi}_1^0 l^\pm)_{\text{tree}}, \quad (26)$$

where the branching ratio of the decay $\tilde{l}_1^\pm \rightarrow \tilde{\chi}_1^0 l^\pm$ is defined by

$$Br(\tilde{l}_1^\pm \rightarrow \tilde{\chi}_1^0 l^\pm)_{\text{tree}} = \frac{\Gamma(\tilde{l}_1^\pm \rightarrow \tilde{\chi}_1^0 l^\pm)_{\text{tree}}}{\Gamma_{\tilde{l}_1}^{\text{tree}}}. \quad (27)$$

The feature that the single-pole approximation reproduces the $\tilde{\chi}_2^0$ partial width can be seen from the identity

$$\int_{-\infty}^{\infty} dk^2 \frac{1}{\left| k^2 - m_{\tilde{l}_1}^2 + i\Gamma_{\tilde{l}_1}^{\text{tree}} m_{\tilde{l}_1} \right|^2} = \frac{\pi}{m_{\tilde{l}_1} \Gamma_{\tilde{l}_1}^{\text{tree}}}. \quad (28)$$

If $\Gamma_{\tilde{l}_1}^{\text{tree}} \ll m_{\tilde{l}_1}$ the integral in (28) will be dominated by the regions of k^2 close to $m_{\tilde{l}_1}^2$, i.e. only a narrow range of k^2 will contribute significantly. Moreover, the squared $V_{\tilde{l}_1^\pm \tilde{\chi}_1^0 l^\pm}^{\text{tree}}$ is proportional to the $\tilde{l}_1^\pm \rightarrow \tilde{\chi}_1^0 l^\pm$ partial width; together with the factor $1/\Gamma_{\tilde{l}_1}^{\text{tree}}$ from (28) this reproduces the factor $Br(\tilde{l}_1^\pm \rightarrow \tilde{\chi}_1^0 l^\pm)$ in (26).

Here we concentrate on scenarios where only the lighter charged sleptons \tilde{l}_1 can be produced in $\tilde{\chi}_2^0$ decays; scenarios where sneutrinos and/or heavier charged sleptons can also be produced in two-body decays of $\tilde{\chi}_2^0$ can be treated analogously.

4 One-loop calculations for $\tilde{\chi}_2^0 \rightarrow \tilde{\chi}_1^0 l^- l^+$

The single-pole approximation can also be used at the one-loop level; however, we will first describe the complete calculation.

4.1 Complete one-loop calculation

4.1.1 Virtual corrections

In general the virtual one-loop corrections to three-body decays can be classified as *self-energy contributions*, *vertex contributions* and *box contributions*. The first two classes are UV finite only after adding the contributions from the counterterms that originate from the renormalization of the MSSM, as discussed in Sec. 2; the box diagrams are by themselves UV finite. The MSSM Feynman rules, as well as the resulting counterterms, are implemented in the FEYNARTS package of computer programs [24], which allows an automated generation of the Feynman diagrams. The matrix element and the one-loop integrals are calculated with the help of the packages FORMCALC and LOOPTOOLS [25], respectively.

Similarly to the tree-level case, diagrams with a slepton \tilde{l}_1 propagator have singularities when \tilde{l}_1 can be on shell. We remove the singularities by introducing a finite width of \tilde{l}_1 as in (21). Following the strategy in Sec. 3, one can obtain a gauge invariant matrix element at one-loop level. In order to obtain $\mathcal{O}(\alpha)$ accuracy near the \tilde{l}_1 resonance, one needs to calculate the complex pole m_p^2 to two-loop level [23],

$$m_p^2 = m_{\tilde{l}_1}^2 - im_{\tilde{l}_1} \Gamma_{\tilde{l}_1}^{1\text{-loop}}, \quad (29)$$

where we have applied the on-shell renormalization scheme at two-loop level, and $\Gamma_{\tilde{l}_1}^{1\text{-loop}}$ denotes the one-loop-level width of \tilde{l}_1 . Then the gauge invariant matrix element at one-loop level can be written as

$$M_{\text{tree}} + M_{\text{virt}} = \frac{A(k^2)}{k^2 - m_{\tilde{l}_1}^2 + im_{\tilde{l}_1} \Gamma_{\tilde{l}_1}^{1\text{-loop}}} + C(k^2), \quad (30)$$

where $C(k^2)$ denotes the non-resonant part of the matrix element, the residue $A(k^2)$ can be expressed as

$$\begin{aligned} A(k^2) = & V_{\tilde{\chi}_2^0 \tilde{l}_1^\pm l^\mp}^{\text{tree}}(k^2) V_{\tilde{l}_1^\pm \tilde{\chi}_1^0 l^\pm}^{\text{tree}}(k^2) \left(1 - \frac{\text{Re} \hat{\Sigma}(k^2)}{k^2 - m_{\tilde{l}_1}^2} \right) + \\ & V_{\tilde{\chi}_2^0 \tilde{l}_1^\pm l^\mp}^{\text{tree}}(k^2) \hat{V}_{\tilde{l}_1^\pm \tilde{\chi}_1^0 l^\pm}^{1\text{-loop}}(k^2) + \hat{V}_{\tilde{\chi}_2^0 \tilde{l}_1^\pm l^\mp}^{1\text{-loop}}(k^2) V_{\tilde{l}_1^\pm \tilde{\chi}_1^0 l^\pm}^{\text{tree}}(k^2), \end{aligned} \quad (31)$$

where $\hat{V}_{\tilde{\chi}_2^0 \tilde{l}_1^\pm l^\mp}^{1\text{-loop}}$ and $\hat{V}_{\tilde{l}_1^\pm \tilde{\chi}_1^0 l^\pm}^{1\text{-loop}}$ represent the renormalized one-loop corrections to the $\tilde{\chi}_2^0 \tilde{l}_1^\pm l^\mp$ and $\tilde{l}_1^\pm \tilde{\chi}_1^0 l^\pm$ vertices, respectively.

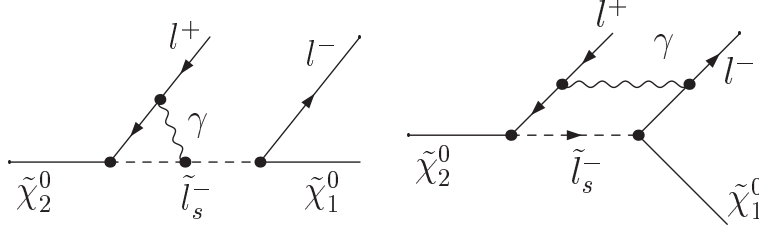


Figure 2: Examples for the virtual photonic corrections

Feynman diagrams like those shown in Fig. 2 also give singularities when the sleptons \tilde{l}_1 are on shell. The left (vertex) diagram has an infrared (IR) divergence if a real slepton mass is used in kinematic configurations where the slepton can be on shell. The right (box) diagram has a divergence which can be understood as being due to re-scattering of the two charged leptons in the final state, which persists for large photon virtualities. One should therefore use complex slepton masses,

$$\frac{1}{k^2 - m_{\tilde{l}_1}^2} \longrightarrow \frac{1}{k^2 - m_{\tilde{l}_1}^2 + im_{\tilde{l}_1} \Gamma_{\tilde{l}_1}^{1\text{-loop}}} \quad (32)$$

in the one-loop integrals from these diagrams. This gives rise to a large QED logarithm $\log(m_{\tilde{l}_1}/\Gamma_{\tilde{l}_1}^{1\text{-loop}})$. Furthermore, the box diagram shown in Fig. 2 has the property that the virtual photon is attached to external on-shell charged particles. This results in IR divergences, which we regularized by introducing a fictitious photon mass λ . The IR divergences cancel after we add contributions from real photon bremsstrahlung, which will be discussed in Sec. 4.1.2. The one-loop integrals with complex masses can be calculated with the help of LOOPTOOLS. The analytical expressions for scalar three-point and four-point functions with real arguments can be found in Refs. [21, 26, 27]. We generalized these to allow for complex arguments. Note that in our calculation the masses of the light leptons, i.e. m_l ($l = e, \mu$), are neglected except when they appear in the one-loop integrals, while the τ mass m_τ is kept everywhere.

4.1.2 Real photon bremsstrahlung

In order to cancel the IR divergences in the virtual corrections, we have to add contributions from real photon bremsstrahlung, which contain on-shell propagators of *stable* particles in the limit where the scalar product of the 4-momenta of the photon and the emitting charged particle vanishes.

This always happens, regardless of the mass of the emitting particle, if the photon energy E_γ is very small. The “soft photon bremsstrahlung” contribution is defined via the condition $E_\gamma \leq \Delta E$; here the cutoff parameter ΔE should be small compared to the relevant physical energy scale (e.g. the resolution of the experimental apparatus). This IR-divergent contribution is sufficient to cancel the IR divergences from the virtual

corrections. Since the energy of the emitted soft photon is by definition very small, this emission essentially does not change the momenta of the other final state particles. This contribution is therefore described as a convolution of the differential tree-level decay width with a universal factor. Explicit expressions can be found in Refs. [21, 26].

Real emission contributions with $E_\gamma > \Delta E$ are called “hard photon bremsstrahlung”. Altogether,

$$\Gamma_{\text{brems}} = \Gamma_{\text{soft}}(\Delta E) + \Gamma_{\text{hard}}(\Delta E). \quad (33)$$

The dependence on the largely arbitrary parameter ΔE cancels after summing soft and hard contributions, provided it is sufficiently small. In the limit of vanishing mass of the emitting particle, the hard photon bremsstrahlung contribution also contains a divergence, if the momenta of the photon and the emitting particle are collinear. Since there are no massless charged particles in Nature, this is not a real divergence; in our case, it is regularized by the masses of the leptons in the final state. However, since the lepton masses, i.e. m_e and m_μ , are very small, it is very difficult to get stable numerical results from a direct numerical evaluation of hard photon bremsstrahlung, e.g. using Monte Carlo integration.

This can be overcome by dividing hard photon bremsstrahlung into a collinear part, where the angle between the photon and the radiating particle is smaller than a very small angle $\Delta\theta$, and the complementary non-collinear part,

$$\Gamma_{\text{hard}}(\Delta E) = \Gamma_{\text{coll}}(\Delta E, \Delta\theta) + \Gamma_{\text{non-coll}}(\Delta E, \Delta\theta). \quad (34)$$

The angular cutoff $\Delta\theta$ should be so small that the emission of photons emitted at angle $\theta < \Delta\theta$ relative to the emitting lepton can be assumed not changing the *direction* of the 3-momentum of this lepton.

If we treat a charged lepton and a collinear photon inclusively, i.e. the momentum of collinear photon is added to that of the emitting lepton, analytically the differential contribution of the collinear emissions is written as the differential tree-level decay width multiplied by a universal function [28, 29]. This approach is for collinear-safe observables [29]. If one adds the soft and collinear contributions to the virtual corrections, all singularities ($\ln m_l$ and $\ln \lambda$) cancel. This is in accordance with the Kinoshita-Lee-Nauenberg theorem [30]. At the LHC the electron energy is determined calorimetrically: in this case a collinear photon would hit the same cell of the calorimeter as the lepton, so the two energies cannot be disentangled.³ Hence the electron observables are defined as collinear-safe observables in our calculation.

We also consider non-collinear-safe observables [29], where the lepton and its collinear photon are not treated inclusively. The contribution of the collinear photon bremsstrahlung cannot be calculated analytically. In this case the mass singularity $\ln m_l$ cannot be canceled

³There is a minor caveat to this statement. The experimental definition of an “electron” usually requires the existence of a charged track whose energy - more exactly, absolute three-momentum - should not be grossly different from the energy measured by the calorimeter. This requirement may remove a few events with very hard collinear photons.

in the differential width and hence becomes visible. Muon energies are generally measured through the curvature of their track in a magnetic field. This measures the energy (more exactly, the 3-momentum) of the muon *after* emitting the collinear photon (if any). In our calculation the muon observables are treated as non-collinear-safe observables. Finally, the contribution from the emission of hard non-collinear photons is calculated by using a multi-channel Monte Carlo approach [31].

The virtual photonic corrections by themselves are UV divergent⁴, hence one cannot meaningfully separate the QED corrections from the one-loop contributions by simply selecting diagrams which contain a photon. In the case of the light lepton ($l = e, \mu$) final states, following conventions of the Supersymmetric Parameter Analysis (SPA) [32], we can pick out and separate potentially large QED terms from the the sum of virtual and soft photon bremsstrahlung corrections, $\Gamma_{\text{virt}} + \Gamma_{\text{soft}}$:

$$\Gamma_{\text{virt}} + \Gamma_{\text{soft}} = \tilde{\Gamma} + \Gamma_{\text{remainder}} , \quad (35)$$

where $\tilde{\Gamma}$ contains all the potentially large terms proportional to $\log m_l$ or $\log \Delta E$, while $\Gamma_{\text{remainder}}$ is IR and UV finite and free of such large QED logarithms. The “QED contributions” can then be defined as follows:

$$\Gamma_{\text{QED}} = \tilde{\Gamma} + \Gamma_{\text{hard}} . \quad (36)$$

Note that Γ_{QED} defined in this way does not depend on the cutoff parameters ΔE and $\Delta\theta$. Moreover, terms proportional to $\log m_l$ cancel between the two contributions in Γ_{QED} in (36) (specifically, between $\tilde{\Gamma}$ and Γ_{coll}) in the integrated width and in the differential width for the collinear-safe observables. Using the definitions (35) and (36), the complete one-loop contribution can be written as

$$\begin{aligned} \Gamma_{1\text{-loop}} &= \Gamma_{\text{tree}} + \Gamma_{\text{virt}} + \Gamma_{\text{brems}} \\ &= \Gamma_{\text{tree}} + \Gamma_{\text{remainder}} + \Gamma_{\text{QED}} . \end{aligned} \quad (37)$$

One should perform the replacement (32) also in the real photon bremsstrahlung when the sleptons \tilde{l}_1 can be on shell. In this case $\tilde{\Gamma}$ contains the large QED logarithm $\log(m_{\tilde{l}_1}/\Gamma_{\tilde{l}_1}^{1\text{-loop}})$, besides $\log m_l$ and $\log \Delta E$. However, in the integrated partial width these terms nearly cancel after summing all contributions; more exactly, the total pre-factor of $\log(m_{\tilde{l}_1}/\Gamma_{\tilde{l}_1}^{1\text{-loop}})$ vanishes when $\Gamma_{\tilde{l}_1}^{1\text{-loop}} \rightarrow 0$, once one includes the fact that the squared $\tilde{l}_1^\pm \tilde{\chi}_1^0 l^\mp$ vertex is $\propto \Gamma_{\tilde{l}_1}$.⁵

When $\tau^- \tau^+$ are the final states of $\tilde{\chi}_2^0$ decay, the τ mass m_τ is kept everywhere. This mass is so large that a stable numerical result can be obtained from the hard photon bremsstrahlung even for $\Delta\theta \rightarrow 0$, i.e. we do not need to divide the hard photon

⁴In principle one can define a renormalizable non-supersymmetric theory containing only leptons, sleptons, neutralinos and photons. However, the counterterms computed in this theory would be different from those of the full MSSM.

⁵In the limit $\Gamma_{\tilde{l}_1} \rightarrow 0$ some kinematical distributions would become singular; for example, the distribution in the invariant mass of the $\tilde{\chi}_1^0 - l^\pm$ systems would contain δ -functions.

bremsstrahlung contribution into collinear and non-collinear parts. Since we do not count terms $\propto \log m_\tau$ as a “large logarithm”, we follow a slightly different procedure to define the “QED part” of the correction. The virtual corrections contain photonic and non-photonic contributions,

$$\Gamma_{\text{virt}} = \Gamma_{\text{virt}}^\gamma + \Gamma_{\text{virt}}^{\text{non-}\gamma}, \quad (38)$$

both of which are UV divergent, while the sum is finite (after including all counterterms). The photonic virtual corrections can be split into an UV-finite part $\tilde{\Gamma}$ and an UV-divergent part $\Gamma_{\text{UV-div}}^\gamma$,

$$\Gamma_{\text{virt}}^\gamma = \tilde{\Gamma} + \Gamma_{\text{UV-div}}^\gamma. \quad (39)$$

Here $\Gamma_{\text{UV-div}}^\gamma$ contains the terms that would be subtracted in an \overline{DR} regularization of $\Gamma_{\text{virt}}^\gamma$. After this rearrangement, the virtual corrections can be written as

$$\begin{aligned} \Gamma_{\text{virt}} &= \tilde{\Gamma} + \Gamma_{\text{UV-div}}^\gamma + \Gamma_{\text{virt}}^{\text{non-}\gamma} \\ &= \tilde{\Gamma} + \Gamma_{\text{remainder}}, \end{aligned} \quad (40)$$

where $\Gamma_{\text{remainder}} = \Gamma_{\text{UV-div}}^\gamma + \Gamma_{\text{virt}}^{\text{non-}\gamma}$ as well as $\tilde{\Gamma}$ are UV finite. The “QED corrections” are finally defined as

$$\Gamma_{\text{QED}} = \tilde{\Gamma} + \Gamma_{\text{brems}}, \quad (41)$$

where Γ_{brems} stands for the contribution from all diagrams with real photon emission. By construction, Γ_{QED} is both UV and IR finite.

4.2 One-loop calculation in the single-pole approximation

If $\tilde{\chi}_2^0 \rightarrow \tilde{l}_1 l$ two-body decays are allowed and $\tilde{\chi}_2^0$ does not have other two-body decay modes, at one-loop level, just like at tree level, the decays $\tilde{\chi}_2^0 \rightarrow \tilde{\chi}_1^0 l^- l^+$ can be approximately treated as production and decay of the sleptons \tilde{l}_1 ,

$$\Gamma(\tilde{\chi}_2^0 \rightarrow \tilde{\chi}_1^0 l^- l^+)_{1\text{-loop}} \simeq \Gamma(\tilde{\chi}_2^0 \rightarrow \tilde{l}_1^\pm l^\mp)_{1\text{-loop}} Br(\tilde{l}_1^\pm \rightarrow \tilde{\chi}_1^0 l^\pm)_{1\text{-loop}}, \quad (42)$$

with

$$Br(\tilde{l}_1^\pm \rightarrow \tilde{\chi}_1^0 l^\pm)_{1\text{-loop}} = \frac{\Gamma(\tilde{l}_1^\pm \rightarrow \tilde{\chi}_1^0 l^\pm)_{1\text{-loop}}}{\Gamma_{\tilde{l}_1}^{1\text{-loop}}}. \quad (43)$$

The virtual contributions of the production and decay of the sleptons \tilde{l}_1 , which now only contain vertex type corrections but no box diagrams, are again calculated with the help of the programs FEYNARTS, FORMCALC and LOOPTOOLS. In order to obtain IR-finite results, the real photon bremsstrahlung is added, which is again separated into an IR-divergent soft part and an IR-finite hard part. For the light lepton final states $l = e, \mu$,

the division of the hard photon bremsstrahlung contribution into a collinear part, which can be calculated analytically, and a non-collinear part, which is calculated numerically, proceeds along the lines described in Sec. 4.1.2. As discussed in Sec. 4.1, the UV-divergent photonic contributions cannot be treated separately as “QED corrections”. We define the “QED corrections” in the same way as in the complete calculation. One finally arrives at a total one-loop contribution which is independent of the cutoff parameters.

5 Total decay width of $\tilde{\chi}_2^0$ and the branching ratios of the decays $\tilde{\chi}_2^0 \rightarrow \tilde{\chi}_1^0 l^- l^+$

As discussed in Sec. 1, the next-to-lightest neutralino $\tilde{\chi}_2^0$ can decay into the LSP $\tilde{\chi}_1^0$ and two fermions $f\bar{f}$. The leptonic final states are important because they can be identified at the LHC. Moreover, the endpoint of the dilepton invariant mass distribution is used to determine the mass relations of supersymmetric particles. The invisible $\tilde{\chi}_2^0$ decay modes, i.e. $\tilde{\chi}_2^0 \rightarrow \tilde{\chi}_1^0 \nu_l \bar{\nu}_l$, do not effect the dilepton invariant mass distribution. But they contribute to the total width of $\tilde{\chi}_2^0$. Since it is very difficult to identify quarks at the LHC, the hadronic decays $\tilde{\chi}_2^0 \rightarrow \tilde{\chi}_1^0 q\bar{q}$ are less interesting than leptonic decays. In order to obtain the total decay width of $\tilde{\chi}_2^0$, these hadronic decays must be calculated. The total decay width of $\tilde{\chi}_2^0$ can be written as

$$\Gamma_{\tilde{\chi}_2^0} = \sum_{l=e,\mu,\tau} \left[\Gamma(\tilde{\chi}_2^0 \rightarrow l^- l^+ \tilde{\chi}_1^0) + \Gamma(\tilde{\chi}_2^0 \rightarrow \nu_l \bar{\nu}_l \tilde{\chi}_1^0) \right] + \sum_{q=u,d,c,s,b} \Gamma(\tilde{\chi}_2^0 \rightarrow q\bar{q} \tilde{\chi}_1^0). \quad (44)$$

Here we assume that the decay $\tilde{\chi}_2^0 \rightarrow \tilde{\chi}_1^0 t\bar{t}$ is not kinematically allowed. The branching ratios of the leptonic decays $\tilde{\chi}_2^0 \rightarrow \tilde{\chi}_1^0 l^+ l^-$ are defined as

$$Br(\tilde{\chi}_2^0 \rightarrow \tilde{\chi}_1^0 l^+ l^-) = \frac{\Gamma(\tilde{\chi}_2^0 \rightarrow \tilde{\chi}_1^0 l^+ l^-)}{\Gamma_{\tilde{\chi}_2^0}}. \quad (45)$$

The invisible decays $\tilde{\chi}_2^0 \rightarrow \tilde{\chi}_1^0 \nu_l \bar{\nu}_l$ are calculated at tree and one-loop level. At tree level these decays can proceed through the exchange of sneutrinos or Z bosons; cf. Fig. 1. Here we focus on the case where the decays $\tilde{\chi}_2^0 \rightarrow \tilde{\chi}_1^0 \nu_l \bar{\nu}_l$ are pure three-body decays. These decays are calculated similarly to the calculations for the leptonic three-body decays $\tilde{\chi}_2^0 \rightarrow \tilde{\chi}_1^0 l^- l^+$. Since none of the external particles carries electric charge in the decays $\tilde{\chi}_2^0 \rightarrow \tilde{\chi}_1^0 \nu_l \bar{\nu}_l$, there are no corrections involving real or virtual photons, and hence no IR divergences. Therefore, there are also no QED corrections in these decays. This makes the calculation of the partial width into neutrinos considerably simpler than for decays into charged leptons.

The hadronic decays of $\tilde{\chi}_2^0$ are calculated in order to obtain the total width of $\tilde{\chi}_2^0$. The Born Feynman diagrams for the decays $\tilde{\chi}_2^0 \rightarrow \tilde{\chi}_1^0 q\bar{q}$ ($q \neq t$) are similar to those of Fig. 1 with intermediate squarks instead of sleptons. Here we only consider the case where the hadronic decays $\tilde{\chi}_2^0 \rightarrow \tilde{\chi}_1^0 q\bar{q}$ are pure three-body decays. Since the SUSY-QCD corrections are not considered in our calculations, these decays can be treated in the same way as

$\tilde{\chi}_2^0 \rightarrow \tilde{\chi}_1^0 l^- l^+$. The virtual photonic corrections of the hadronic decays (the diagrams are similar to the ones of the leptonic decays, i.e. Fig. 2) are IR divergent. The contributions of the real photon bremsstrahlung are necessary for the cancellation of the IR divergences. We neglect the light quark masses, i.e. $m_q (q = u, d, s)$, except when they appear in the one-loop integrals. In analogy to Sec. 4.1.2, the contributions of the real photon bremsstrahlung are also splitted into an IR-divergent soft part and an IR-finite hard part. For the light quark final states, we separate the hard photon bremsstrahlung into a collinear part and a non-collinear part in order to obtain stable numerical results. Since quarks are detected as jets, which contain many photons, quark energies are always collinear-safe. As presented in Sec. 4.1.2, the soft and collinear contributions are calculated analytically. We treat the decays with heavy quark final states in the same way as $\tau^- \tau^+$ final states. The QED corrections are defined in the same way as in Sec. 4.1.2 since the photonic contributions are UV divergent and cannot be treated separately.

6 Numerical results and discussion

We are now ready to present numerical results of our calculation. We present results both for a scenario where $\tilde{\chi}_2^0$ can undergo two-body decays, and for a scenario where no two-body decays of $\tilde{\chi}_2^0$ are possible. Furthermore, we discuss both the integrated partial widths and branching ratios of $\tilde{\chi}_2^0$, and the distribution of the $l^+ l^-$ invariant mass; this distribution is of great interest for future experiments, as discussed in the Introduction. Since we always assume equal masses for selectrons and smuons and the light lepton mass m_l ($l = e, \mu$) is neglected except when it appears in the one-loop integrals, the integrated partial widths for the $e^+ e^- \tilde{\chi}_1^0$ and $\mu^+ \mu^- \tilde{\chi}_1^0$ final states are identical. As discussed in Sec. 4.1.2, the dilepton invariant mass $M_{e^+e^-}$ is defined as collinear-safe observable, i.e. we add the momentum of a collinear photon to that of the emitting electron, since it is difficult to separate their energies at the LHC. The energies of a muon and its collinear photon can be disentangled easily at the LHC, hence the dilepton invariant mass $M_{\mu^+\mu^-}$ is defined as non-collinear-safe observable, i.e. the momentum of a collinear photon is not added to that of its emitter muon. In this case the large logarithm $\ln m_\mu$ can not cancel in the distribution, so the mass effect can be seen in the dilepton invariant mass distribution. One will obtain identical $M_{e^+e^-}$ and $M_{\mu^+\mu^-}$ distributions if both of them are defined as collinear-safe observables. In order to see the differences of the two treatments (adding and not adding the momentum of a collinear photon to the emitting lepton), we also show the comparison of dilepton invariant mass $M_{\mu^+\mu^-}$ and $M_{e^+e^-}$ distributions.

6.1 Numerical results for the SPS1a parameter set

We first present results for the SPS1a benchmark scenario, as described in Table 1 in the Introduction. The dilepton invariant mass $M_{e^+e^-}$ distribution from the complete calculation is shown in Fig. 3. In the left frame we show not only the tree-level and total one-loop predictions, but also the separate QED and “remainder” corrections, see (37). We see that

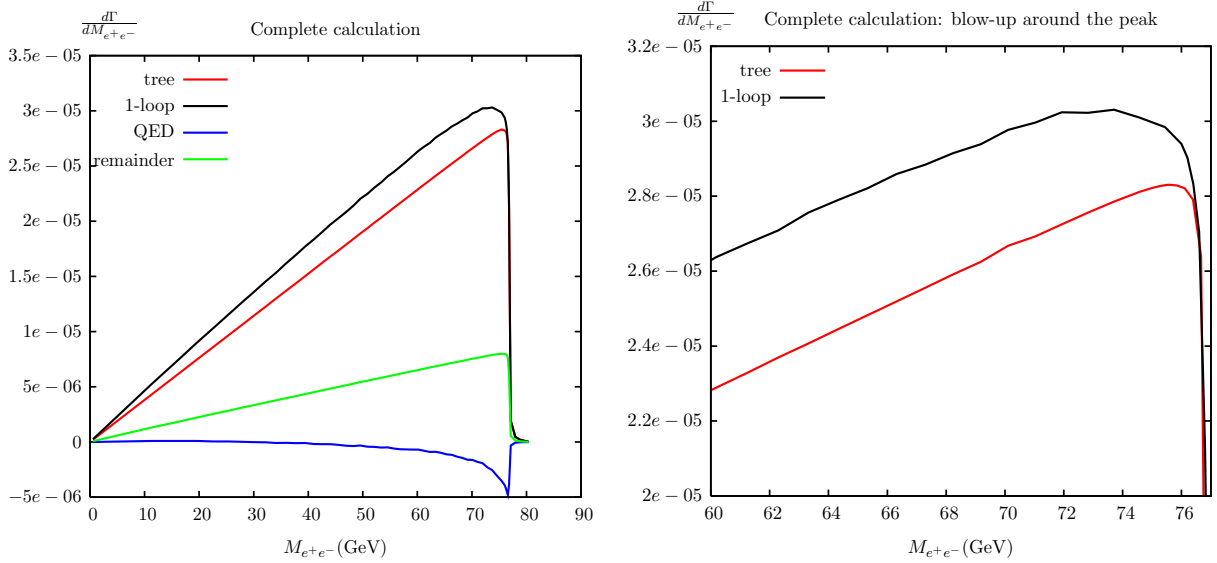


Figure 3: The dilepton invariant mass $M_{e^+e^-}$ distribution for the SPS1a parameter set (complete calculation).

the non-QED contributions are positive and quite large everywhere, whereas the QED contribution is large and negative near the endpoint of the distribution, but small elsewhere. In full three-body kinematics this endpoint is simply given by $M_{e^+e^-}^{\max}|_{3\text{-body}} = m_{\tilde{\chi}_2^0} - m_{\tilde{\chi}_1^0}$. However, for the SPS1a parameter set $\tilde{\chi}_2^0$ decays are dominated by contributions with on-shell \tilde{l}_1 in the intermediate state. The endpoint for this two-body configuration is given by

$$M_{e^+e^-}^{\max}|_{2\text{-body}} = m_{\tilde{\chi}_2^0} \sqrt{1 - \frac{m_{\tilde{e}_1^\pm}^2}{m_{\tilde{\chi}_2^0}^2}} \sqrt{1 - \frac{m_{\tilde{\chi}_1^0}^2}{m_{\tilde{e}_1^\pm}^2}} \simeq 76.8 \text{ GeV}, \quad (46)$$

where the numerical value holds for the SPS1a scenario. Note that this is only 3.6 GeV below the endpoint of the three-body decays. At tree level, the $M_{e^+e^-}$ distribution peaks at the region which is a little below the endpoint of the two-body contribution. The right panel in Fig. 3, which shows a blow-up of the endpoint region, shows that the peak of this distribution is then moved about 4 GeV below the endpoint (46) once higher-order corrections are included. This is almost entirely due to contributions where a hard photon is emitted, which takes away energy from the e^+e^- system. This change of the shape of the invariant mass distribution near the endpoint is important, since in (simulated) experiments one needs a fitting function describing this distribution in order to determine the location of the endpoint [33]. In Fig. 3 we used $\Delta\theta = 1^\circ$ in the definition of collinear photons. In a real experiment, even photons emitted at somewhat larger angles might be counted as contributing to the energy of the emitting electron. In this case the change of the shape of the $M_{e^+e^-}$ distribution will be somewhat smaller.

In Fig. 4 we compare the numerical results of the complete calculation and the single-pole approximation at tree (left) and one-loop level (right). At tree level the $M_{e^+e^-}$ distri-

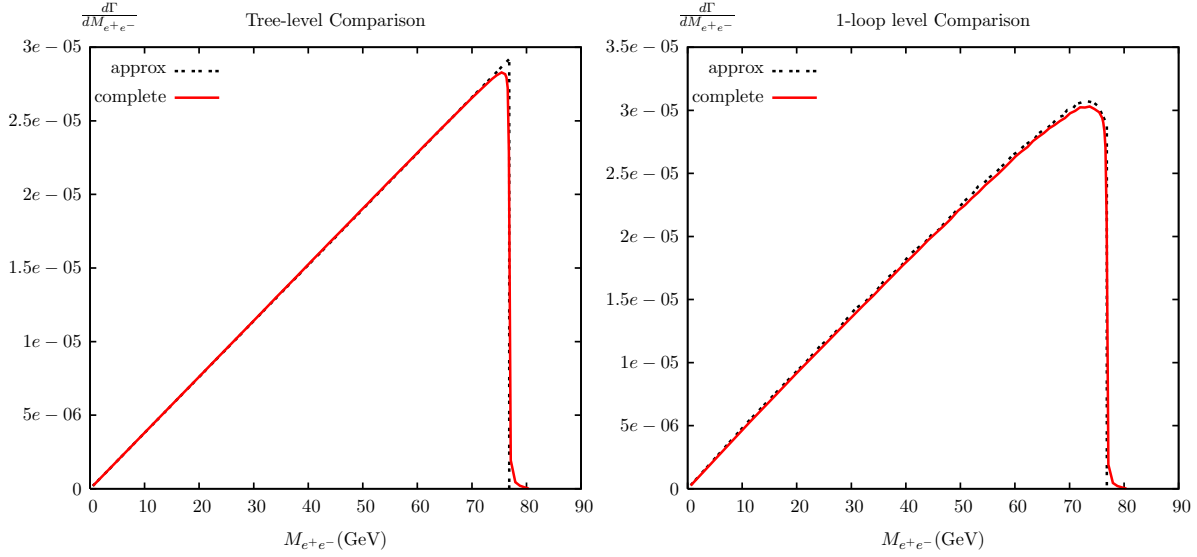


Figure 4: The dilepton invariant mass $M_{e^+e^-}$ distribution for the SPS1a parameter set (comparison of the complete calculation with the approximate calculation).

bution computed in the single-pole approximation has an exactly triangular shape, with a sharp edge at the endpoint (46). This edge is smeared out a bit in the complete tree-level calculation, which includes the full set of diagrams shown in Fig. 1. As noted above, this edge is also softened considerably once hard photon emission is included. The single-pole approximation therefore works even better in the one-loop calculation. However, this excellent agreement even for the differential decay width is partially accidental. The agreement would become somewhat worse if the endpoints in two- and three-body kinematics were further apart; this would happen if the mass of \tilde{l}_1 was close to the mass of either $\tilde{\chi}_2^0$ or to that of $\tilde{\chi}_1^0$, since then one of the two square roots in (46) would become small.

The comparison of the dilepton invariant mass $M_{\mu^+\mu^-}$ and $M_{e^+e^-}$ distributions is shown in Fig. 5. In the upper frames we show the dilepton invariant mass $M_{l^+l^-}$ ($l = e, \mu$) distribution both at tree and one-loop level. Since the selectrons and smuons have equal masses and the light lepton mass m_l ($l = e, \mu$) is neglected except when it appears in the one-loop integrals, their distributions are identical at tree level and different at one-loop level due to the different treatment of the collinear-photon radiation. From these figures one obtains that at one-loop level the mass effect is larger near the endpoint than in other regions and the peak of the $M_{\mu^+\mu^-}$ distribution is shifted to lower invariant-mass values in comparison with the $M_{e^+e^-}$ distribution. We also show the relative one-loop corrections in the lower frames in Fig. 5. The relative one-loop corrections from the $\mu^+\mu^-$ final state is smaller than that of the e^+e^- final state in the upper invariant-mass region, while it is larger in the lower invariant-mass region. The main reason is that we add the momenta of collinear photons to that of emitting electrons, but we do not do this for the collinear-photon radiation from muons. Hence the invariant mass $M_{\mu^+\mu^-}$ is reduced in comparison with $M_{e^+e^-}$. This leads to the shifting of events from the upper invariant-mass region to

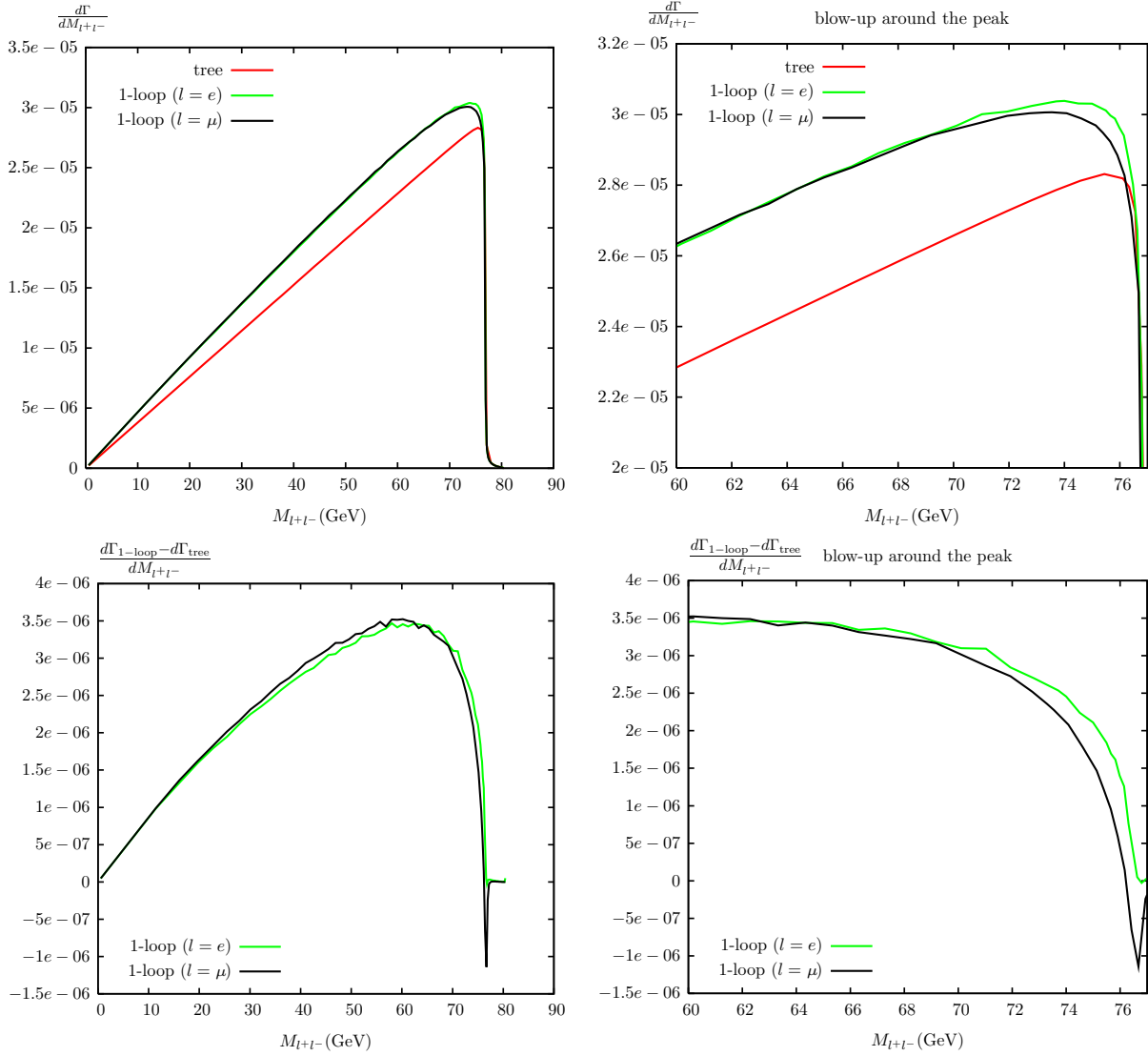


Figure 5: The comparison of the dilepton invariant mass $M_{\mu^+\mu^-}$ and $M_{e^+e^-}$ distribution for the SPS1a parameter set.

the lower invariant-mass region.

The corresponding results for the $\tau^+\tau^-\tilde{\chi}_1^0$ final state are shown in Figs. 6 and 7. Fig. 6 shows that both the QED and, in particular, the non-QED corrections are smaller in magnitude than for light leptons. In case of the QED contribution this is essentially a mass effect. Our angular cutoff $\Delta\theta$ defining the collinear region in (34) is so small that even non-collinear radiation off electrons or muons is still more likely than any hard radiation off τ leptons; recall that we do not split hard radiation into collinear and non-collinear contributions for $\tau^+\tau^-\tilde{\chi}_1^0$ final states.

The reduction of the non-QED corrections is even more dramatic. They amount to about +20% for electrons and muons, but only to about +6% for tau leptons. This

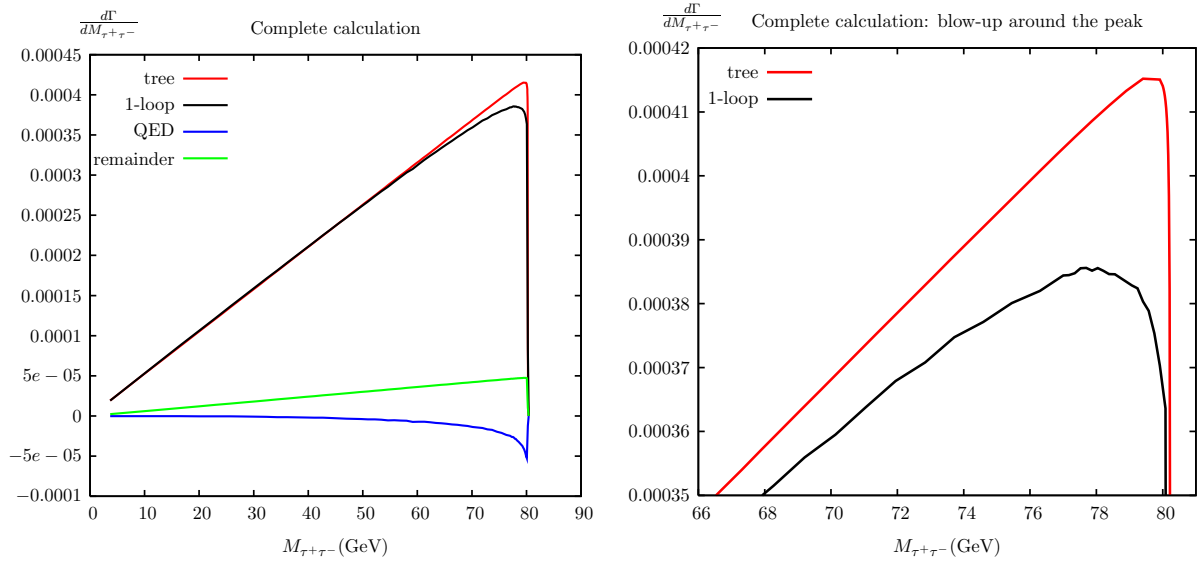


Figure 6: The dilepton invariant mass $M_{\tau^+\tau^-}$ distribution for the SPS1a parameter set (complete calculation).

difference stems from the fact that \tilde{l}_1 is a pure $SU(2)$ singlet for $l = e, \mu$, since we neglect terms $\propto m_l$ in the mass matrices of these sleptons. In contrast, $\tilde{\tau}_L - \tilde{\tau}_R$ mixing is quite significant, leading to a sizable $SU(2)$ doublet component of $\tilde{\tau}_1$. Therefore $\tilde{\chi}_2^0$ decays into (real or virtual) \tilde{l}_1 can only proceed through its small $U(1)_Y$ gaugino (bino) component for $l = e, \mu$, while the large $SU(2)$ gaugino (neutral wino) component also contributes for $l = \tau$. Moreover, the $\tilde{\chi}_1^\pm \tilde{l}_1^\mp \nu_l$ coupling, which is involved in the virtual corrections, only exists for $l = \tau$. The reason is that \tilde{l}_1 is a pure $SU(2)$ singlet for $l = e, \mu$ while $\tilde{\tau}_1$ has a sizeable $SU(2)$ doublet component, as explained above. In the limit of exact SUSY, these contributions involve the $U(1)_Y$ and $SU(2)$ gauge couplings, respectively, which renormalize (and run) quite differently. If there are significant differences between masses of supersymmetric particles, the differences between the true gauge couplings and these gaugino-lepton-slepton couplings also becomes significant [34]; note that in the SPS1a scenario, squarks (which contribute to various two-point functions) are about three times heavier than $\tilde{\chi}_2^0$. Finally, the $\tilde{\chi}_2^0 \tilde{\tau}_1 \tau$ vertex also receives non-negligible contributions which, again in the limit of exact SUSY, are proportional to the τ Yukawa coupling [1]. As a result of the reduced non-QED corrections, the total correction is now *negative*, especially for large values of $M_{\tau^+\tau^-}$.

The endpoint region of the $M_{\tau^+\tau^-}$ distribution from the complete calculation is shown in the right panel of Fig. 6. We see that the peak of the distribution is shifted downwards by about 2 GeV once higher-order corrections are included. A shift of this magnitude may be significant, even though the $\tau^+\tau^-$ invariant mass is in general difficult to measure accurately, due to the presence of ν_τ (anti-)neutrinos in the τ decay products, which escape detection.

In Fig. 7 predictions from the complete calculation are compared to those from the

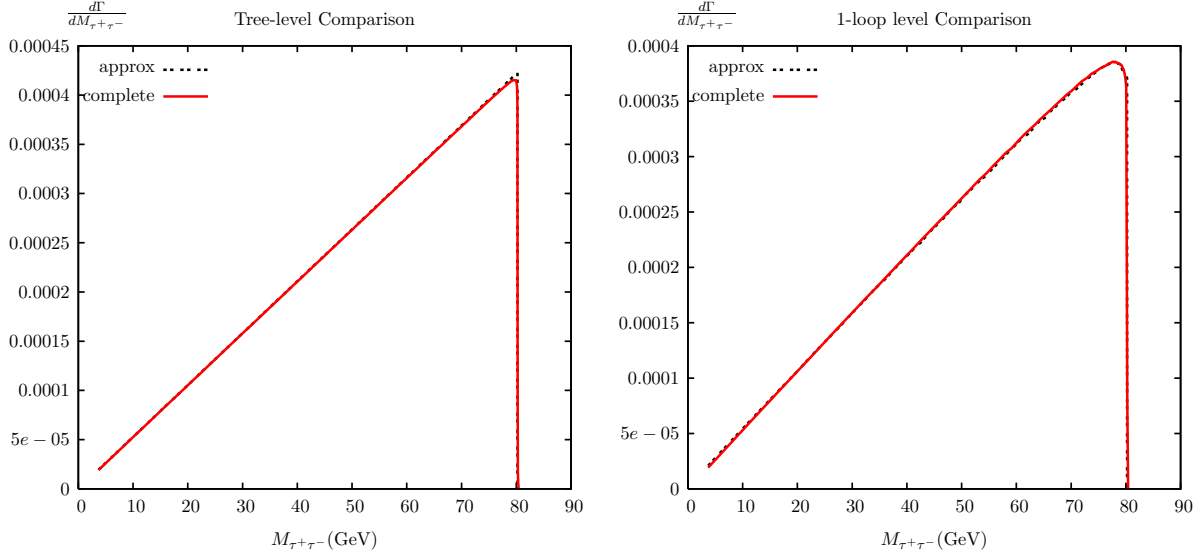


Figure 7: The dilepton invariant mass $M_{\tau^+\tau^-}$ distribution for the SPS1a parameter set (comparison of the complete calculation with the approximate calculation).

single-pole approximation. In this case we find almost perfect agreement even in the endpoint region, both at tree level and after including one-loop corrections. The reason is that for SPS1a, $m_{\tilde{\tau}_1}$ happens to be very close to $\sqrt{m_{\tilde{\chi}_1^0} m_{\tilde{\chi}_2^0}}$. Performing the replacement $m_{\tilde{e}_1} \rightarrow m_{\tilde{\tau}_1}$ in (46) shows that the endpoints of the $\tau^+\tau^-$ distributions in two- and three-body kinematics practically coincide.

The partial widths of the different $\tilde{\chi}_2^0$ decay modes and the branching ratios of its visible leptonic decays are listed in Table 2, where the numbers in the parentheses are obtained from the approximate calculations. We find $\sum_l \Gamma(\tilde{\chi}_2^0 \rightarrow \tilde{\chi}_1^0 \nu_l \bar{\nu}_l) \ll \sum_l \Gamma(\tilde{\chi}_2^0 \rightarrow \tilde{\chi}_1^0 l^+ l^-)$. This is not surprising, since the charged lepton final state is accessible via on-shell \tilde{l}_1

decay mode	tree-level width(MeV),	Br	one loop-level width(MeV),	Br
$e^- e^+ \tilde{\chi}_1^0$	1.123 (1.122),	5.9%	1.297 (1.294),	6.7%
$\mu^- \mu^+ \tilde{\chi}_1^0$	1.123 (1.122),	5.9%	1.297 (1.294),	6.7%
$\tau^- \tau^+ \tilde{\chi}_1^0$	16.870 (16.933),	88.0%	16.595 (16.646),	86.2%
$\nu_e \bar{\nu}_e \tilde{\chi}_1^0$	0.012		0.012	
$\nu_\mu \bar{\nu}_\mu \tilde{\chi}_1^0$	0.012		0.012	
$\nu_\tau \bar{\nu}_\tau \tilde{\chi}_1^0$	0.013		0.013	
$q\bar{q} \tilde{\chi}_1^0$ ($q \neq t$)	0.015		0.015	
total width	19.168		19.241	

Table 2: Partial widths of different $\tilde{\chi}_2^0$ decay modes and the branching ratios of its visible decays for the SPS1a parameter set. The numbers in parentheses give the corresponding partial widths calculated in the single-pole approximation.

intermediate state, whereas for the neutrino final state all exchanged particles are off shell. Since squark masses are near 500 GeV in SPS1a scenario, hadronic final states contribute even less than neutrinos do.

From the results in Table 2 one concludes:

- The main decay mode of $\tilde{\chi}_2^0$ is $\tilde{\chi}_2^0 \rightarrow \tau^- \tau^+ \tilde{\chi}_1^0$. Its branching ratio is about 88.0% at tree-level, 86.2% at one-loop level. This mode dominates partly because of the lower mass of $\tilde{\tau}_1$ as compared to \tilde{e}_1 (133.0 GeV vs 142.7 GeV). Even more important is that the $\tilde{\chi}_2^0 \tilde{\tau}_1 \tau$ coupling is much stronger than the $\tilde{\chi}_2^0 \tilde{e}_1 e$ coupling, which in turn is due to significant $L - R$ mixing, which only exists in the $\tilde{\tau}$ sector, as explained above.
- The total $\tilde{\chi}_2^0$ decay width is enhanced by 0.4% when one-loop corrections are included. Such modest corrections are typical in the absence of large enhancement factors (e.g., large logarithms). This overall perturbative stability confirms that our choice of renormalization scheme, and of the electroweak input parameters listed in Appendix A, is indeed rather well suited for the task at hand.⁶
- One-loop corrections enhance the partial width and the branching ratio of $\tilde{\chi}_2^0 \rightarrow l^- l^+ \tilde{\chi}_1^0$ ($l = e, \mu$) decays by 15.5% and 13.6%, respectively. This results from the large size of the positive non-QED corrections depicted in Fig. 3. Much of these corrections can probably be absorbed into an appropriately defined running $\tilde{\chi}_2^0 \tilde{l}_1 l$ coupling. This is illustrated in Fig. 8, which compares the M_{l+l^-} distribution computed including only the “universal corrections” defined in Ref. [11] (see also [34]) with the tree-level and full one-loop results. We see that the residual non-universal corrections are relevant only close to the edge of the lepton pair distribution, where real photon emission is most important. Since this result is for a specific scenario, a more comprehensive analysis might be appropriate.
- The single-pole approximation reproduces the integrated partial widths to about 0.3% accuracy. This agreement is even better than in the M_{l+l^-} distribution shown in Figs. 4 and 6. In fact, from (28) and the discussion at the end of Sec. 4.1.2 one might expect better agreement for the integrated partial width than for (some) kinematical distributions.

6.2 Numerical results for pure three-body decays

We also investigated the effect of higher-order corrections on leptonic $\tilde{\chi}_2^0$ decays for a scenario where $\tilde{\chi}_2^0$ does not have any two-body decay modes. To that end we again use the SPS1a parameter set, except that the soft SUSY-breaking parameters in the slepton mass matrix are set to

$$m_{\tilde{l}_L} = 230 \text{ GeV}, \quad m_{\tilde{l}_R} = 183 \text{ GeV}, \quad l = e, \mu, \tau. \quad (47)$$

⁶Of course, the total width after the inclusion of one-loop corrections is scheme independent, up to unknown two-loop correction terms. However, the relative size of the one-loop corrections does depend on the chosen scheme.

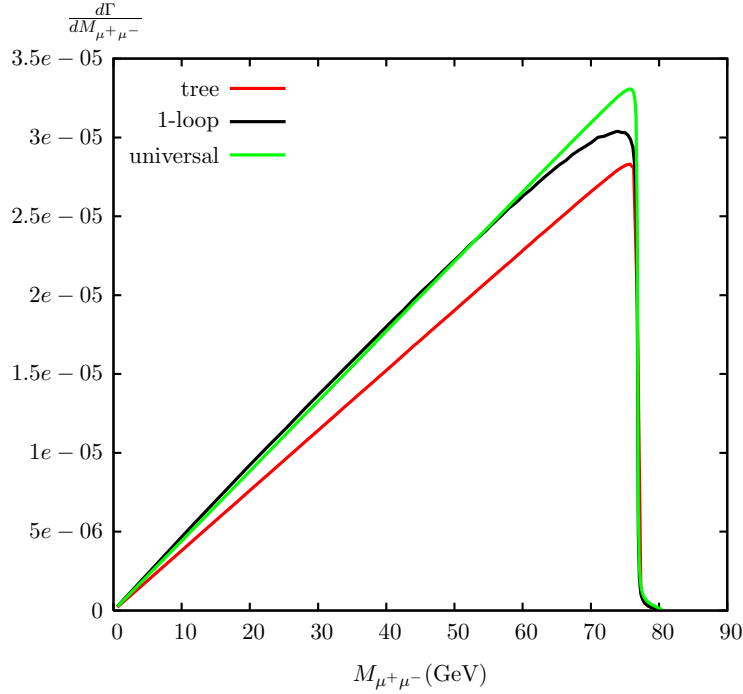


Figure 8: Dilepton invariant mass $M_{\mu^+\mu^-}$ from an approximate calculation with only universal 1-loop contributions via effective couplings, in comparison with the tree-level and the complete 1-loop results. SPS1a parameter set.

The masses of the relevant neutralinos and sleptons in this modified SPS1a parameter set are listed in Table 3 where one finds that $\tilde{\chi}_2^0$ has to undergo a pure three-body decay. Therefore we do not have to introduce complex slepton masses in the one-loop functions. Apart from this simplification, the calculation is very similar to the “complete” calculation described in Sec. 4.1.

particle	$\tilde{\chi}_2^0$	$\tilde{\chi}_1^0$	$\tilde{e}_1 (\tilde{\mu}_1)$	$\tilde{e}_2 (\tilde{\mu}_2)$	$\tilde{\tau}_1$	$\tilde{\tau}_2$	$\tilde{\nu}_l (l = e, \mu, \tau)$
mass (GeV)	176.6	96.2	187.9	234.9	182.3	239.2	221.0

Table 3: Masses of the relevant neutralinos and sleptons for the modified SPS1a parameter set.

The dilepton invariant mass $M_{e^+e^-}$ and $M_{\tau^+\tau^-}$ distributions are shown in Figs. 9 and 10, respectively. At tree level the $M_{e^+e^-}$ distribution shows a small peak near its upper endpoint from the exchange of nearly on-shell Z bosons. Since the QED and non-QED corrections are very small and negative in this region, this peak is less pronounced once one-loop corrections are included. This is of some significance, since the shape of this distribution can now be used to infer the strengths of various contributing diagrams, which in turn provides information on slepton masses and neutralino mixing [8, 35]. Since $\tilde{\tau}$

exchange is much enhanced relative to \tilde{e} exchange, one cannot see any contributions of Z -exchange even at tree level from the $M_{\tau^+\tau^-}$ distribution. Moreover we can observe that the invariant mass $M_{e^+e^-}$ and $M_{\tau^+\tau^-}$ distributions have a rather sharp edge at their endpoints. These edges are again softened by real photon emission, but remain quite distinct. This should facilitate the experimental determination of the endpoint, and hence the measurement of $m_{\tilde{\chi}_2^0} - m_{\tilde{\chi}_1^0}$.

We compare the dilepton invariant mass $M_{\mu^+\mu^-}$ and $M_{e^+e^-}$ distributions in Fig. 11, where the tree- and one-loop-level results, the blow-up of the endpoint region and the relative one-loop corrections are shown. From these figures one obtains that the shapes of the $M_{\mu^+\mu^-}$ and $M_{e^+e^-}$ distributions are identical at tree level and different at one-loop level due to the different treatment of collinear-photon radiations. In contrast to the numerical results from the SPS1a parameter set (see Fig. 5), the mass effect is small in Fig. 11, but it is still distinct, especially in the relative one-loop corrections. In the calculations for the invariant mass distribution, the momentum of a collinear photon is added to that of the emitting electron, but it is not added to that of the emitting muon. Hence the invariant mass $M_{\mu^+\mu^-}$ is reduced in comparison with $M_{e^+e^-}$. It leads to the shifting of events from the upper invariant-mass region to the lower invariant-mass region. This effect can be seen in the lower frames in Fig. 11, i.e. in the lower invariant-mass region the relative one-loop corrections of the $\mu^+\mu^-$ final state is larger than that of e^+e^- final state, while the inverse relation holds in the upper invariant-mass region.

The decay width of different $\tilde{\chi}_2^0$ decay modes and the branching ratios of its visible decays are shown in Table 4. The total $\tilde{\chi}_2^0$ decay width is about 600 times smaller than for scenario SPS1a. This is not surprising, since in this scenario $\tilde{\chi}_2^0$ can only have three-body decays, while the two-body decays $\tilde{\chi}_2^0 \rightarrow \tilde{l}_1^\pm l^\mp \rightarrow \tilde{\chi}_1^0 l^- l^+$ are kinematically allowed in the

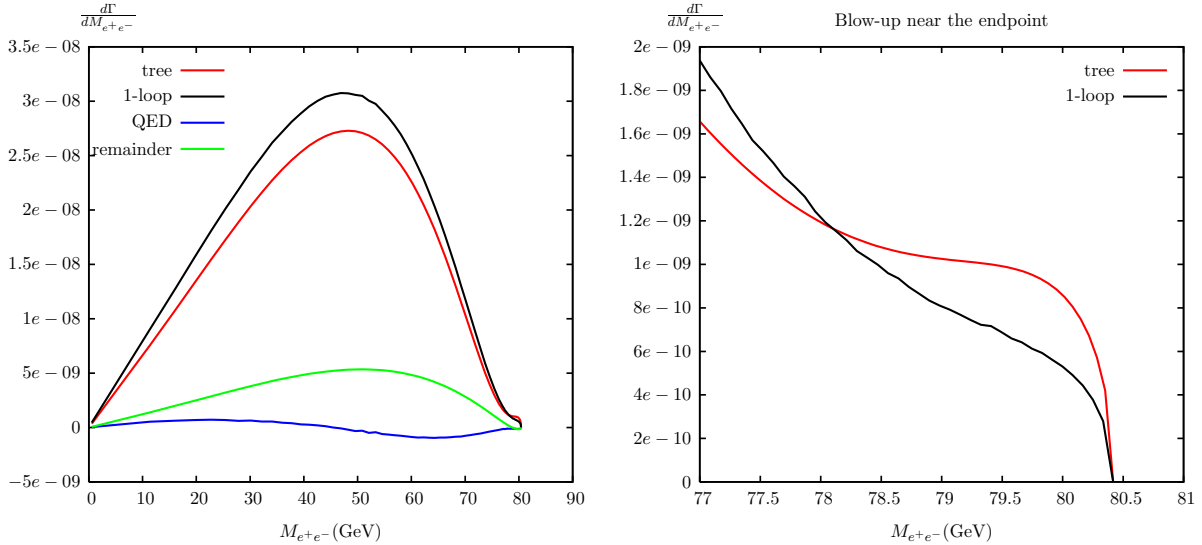


Figure 9: The $\tilde{\chi}_2^0$ decay width differential in the dilepton invariant mass $M_{e^+e^-}$ in the case of genuine three-body decay.

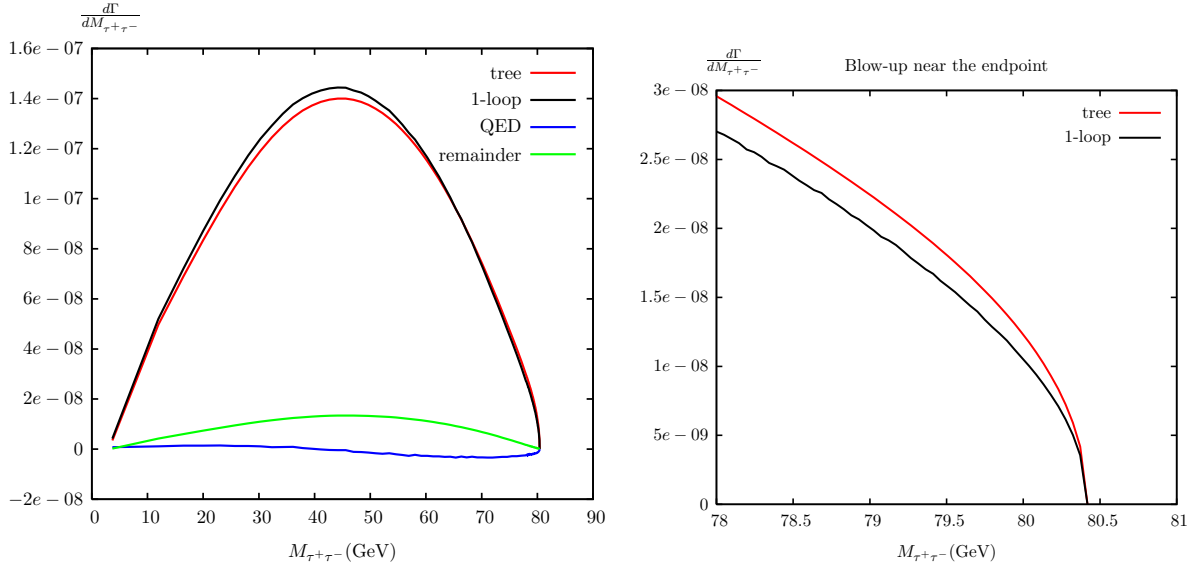


Figure 10: The $\tilde{\chi}_2^0$ decay width differential in the di- τ invariant mass $M_{\tau+\tau-}$ in the case of genuine three-body decay.

scenario SPS1a. In the modified SPS1a scenario one-loop corrections increase the total $\tilde{\chi}_2^0$ decay width by a modest 1.2%.

Turning to the various partial widths of leptonic decays, we notice that the $\tilde{\tau}^+\tilde{\tau}^-\tilde{\chi}_1^0$ final state is still the largest decay mode of $\tilde{\chi}_2^0$ (25.1% at tree level, 25.4% at one-loop level) since $m_{\tilde{\tau}_1}$ is smaller than the selectron and smuon masses and the large $L-R$ mixing exists only in the $\tilde{\tau}$ sector. Note that exchange of the $SU(2)$ doublet sleptons now dominates for $l = e, \mu$ since the size of the $\tilde{\chi}_2^0\tilde{e}_L e$ coupling exceeds that of the $\tilde{\chi}_2^0\tilde{e}_R e$ coupling by nearly a factor of 10 and all the sleptons are off shell in this scenario. This dominance of \tilde{e}_L exchange also explains why the $e^+e^-\tilde{\chi}_1^0$ and $\nu_e\bar{\nu}_e\tilde{\chi}_1^0$ final states now have quite similar partial widths: in the limit where $\tilde{\chi}_2^0$ and $\tilde{\chi}_1^0$ are pure $SU(2)$ and $U(1)_Y$ gauginos, respectively, the product of couplings involved in \tilde{e}_L and $\tilde{\nu}_e$ exchange is exactly the same (up to an overall sign).

The pattern of one-loop corrections to leptonic decays is different from the original SPS1a scenario. The partial width into electrons and muons is still enhanced by about 14.3%. But now the invisible partial widths are also increased, diminishing the correction of the branching ratios. In the original SPS1a scenario, the one-loop partial widths of the invisible decays are almost unchanged in comparison with the tree-level ones, see Table 2. Note that we assumed three exactly degenerate sneutrinos here, unlike in the original SPS1a scenario, where $\tilde{\nu}_\tau$ is slightly lighter than $\tilde{\nu}_e$. In the modified scenario a tiny difference between the partial widths for $\nu_\tau\bar{\nu}_\tau\tilde{\chi}_1^0$ and $\nu_e\bar{\nu}_e\tilde{\chi}_1^0$ final states nevertheless results from one-loop corrections involving the τ mass or Yukawa coupling (e.g. from the $\tilde{\nu}$ and ν two-point functions).

The hadronic final states have very large partial decay widths and branching ratios: $\Gamma_{\text{hadronic}}^{\text{tree}} = 15.210$ keV (52.9%), $\Gamma_{\text{hadronic}}^{1\text{-loop}} = 14.765$ keV (50.7%), though the squark masses are much larger than the slepton masses. Part of the reason is that the Z -exchange dia-

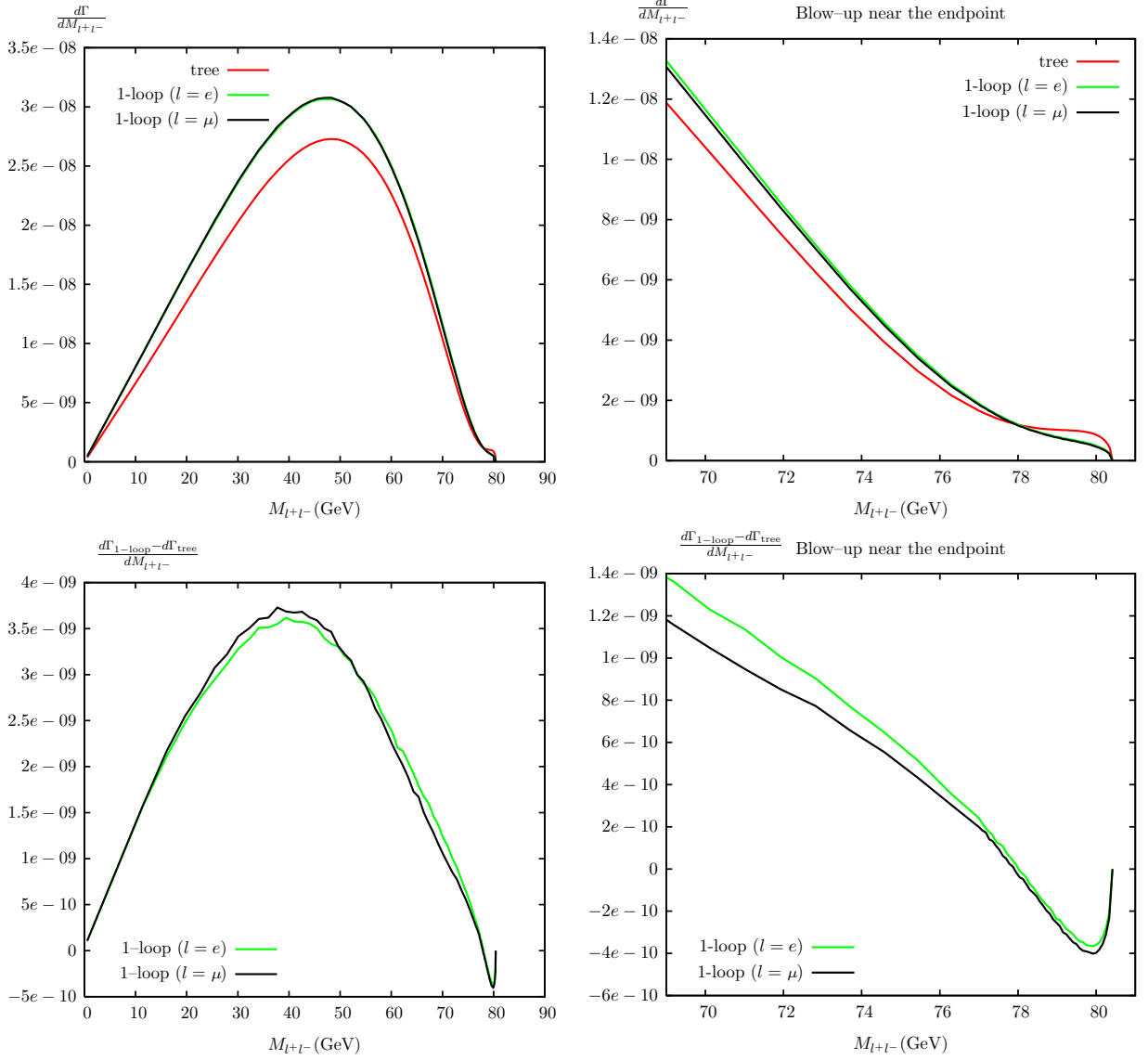


Figure 11: The comparison of the dilepton invariant mass $M_{\mu^+\mu^-}$ and $M_{e^+e^-}$ distribution in the case of a genuine three-body decay.

grams give larger contributions to hadronic final states than to leptonic ones. Moreover, the interference between Z and sfermion exchanges is large and positive for the hadronic final states, while it is also large but negative for the leptonic final states. This is the main reason why the hadronic decays of $\tilde{\chi}_2^0$ obtain so large branching ratios.

decay mode	tree-level width(keV), Br	1loop-level width(keV), Br
$e^-e^+\tilde{\chi}_1^0$	1.270, 4.4%	1.451, 5.0%
$\mu^-\mu^+\tilde{\chi}_1^0$	1.270, 4.4%	1.451, 5.0%
$\tau^-\tau^+\tilde{\chi}_1^0$	7.209, 25.1%	7.383, 25.4%
$\nu_e\bar{\nu}_e\tilde{\chi}_1^0$	1.273	1.355
$\nu_\mu\bar{\nu}_\mu\tilde{\chi}_1^0$	1.273	1.355
$\nu_\tau\bar{\nu}_\tau\tilde{\chi}_1^0$	1.273	1.354
$u\bar{u}\tilde{\chi}_1^0$	2.480	2.386
$d\bar{d}\tilde{\chi}_1^0$	3.330	3.298
$c\bar{c}\tilde{\chi}_1^0$	2.475	2.378
$s\bar{s}\tilde{\chi}_1^0$	3.330	3.298
$b\bar{b}\tilde{\chi}_1^0$	3.595	3.405
total width	28.778	29.114

Table 4: The decay width of different $\tilde{\chi}_2^0$ decay modes and the branching ratios of its visible leptonic decays in the modified SPS1a scenario.

7 Summary and conclusions

We have performed a complete one-loop calculation of the decays $\tilde{\chi}_2^0 \rightarrow l^-l^+\tilde{\chi}_1^0$ ($l = e, \mu, \tau$). The necessary renormalization is briefly described in Sec. 2. In most cases we used on-shell renormalization, which leaves the masses of the relevant neutralinos and sleptons (almost) unchanged. This is convenient for our purpose, since one important goal in the experimental study of leptonic $\tilde{\chi}_2^0$ decays is the determination of (differences of) supersymmetric particles masses from the dilepton invariant mass (M_{l+l^-}) distribution.

For the cases where the intermediate charged sleptons can be on shell, these decays were calculated both completely and in a single-pole approximation at one-loop level. In the complete calculation one has to employ complex slepton masses in the relevant propagators and one-loop integrals. The single-pole approximation in this case is performed in the way that the $\tilde{\chi}_2^0$ decays are treated as a sequence of two two-body decays. We checked that for the well-studied SPS1a parameter set, this approximation reproduces the integrated partial widths to better than 0.5% accuracy even after one-loop corrections are included. For this parameter set we find a rather small one-loop correction to the total $\tilde{\chi}_2^0$ decay width, but the branching ratio for the most easily detectable electron and muon final states are increased by about 13.6% at one-loop level.

We also studied the effect of higher-order corrections on the M_{l+l^-} distribution. If only one exchanged particle can be on-shell, as in the SPS1a scenario, the shape of this distribution is altered only by real photon emission contributions, i.e. its peak is shifted by several GeV below the endpoint. This is very important since the shape of the distribution near the endpoint should be known if the endpoint is to be determined accurately from real data. In our calculation we define collinear photons as being emitted at an angle $\Delta\theta < 1^\circ$

relative to the emitting lepton. Since the selectrons and smuons have equal masses and the light lepton mass m_l ($l = e, \mu$) is neglected except when it appears in the one-loop integrals, one will obtain identical distributions for $M_{e^+e^-}$ and $M_{\mu^+\mu^-}$ if the momentum of a collinear photon is added to that of the emitting lepton. The actual effect of the collinear-photon radiation depends on details of the measurement apparatus, and therefore has to be calculated anew for each experiment. We have focused on the LHC experiment in our calculation. At the LHC the electron energy is determined calorimetrically. In this case a collinear photon would hit the same cell of the calorimeter as the electron, so the two energies cannot be disentangled. Hence we add the momentum of a collinear photon to the one of the emitting electron in our calculation. Since muons pass through the calorimeter, where the photons are detected, and measured further outside in the muon detector at the LHC (their 3-momenta are measured through the curvature radius of their track in the magnetic field), the momentum of a collinear photon is not added to the one of its emitter muon in our calculation. In this case the mass effect can be seen in the dilepton invariant mass distribution. We find that the peak of the $M_{e^+e^-}$ distribution is moved downwards by about 4 GeV once the one-loop corrections are added. In comparison to the $M_{e^+e^-}$ distribution, the peak of the $M_{\mu^+\mu^-}$ distribution is shifted slightly to lower invariant-mass values at one-loop level. This is due to the different treatment of the collinear-photon radiation.

We have also analyzed a modified SPS1a scenario, with increased slepton masses, so that $\tilde{\chi}_2^0$ can only undergo genuine three-body decays. In this case we again find a moderate, if slightly larger, correction to the total $\tilde{\chi}_2^0$ width when one-loop corrections are considered, but the branching ratios for the electron and muon final states are still enhanced by about 13.6% at the one-loop level. We have seen in Fig. 8 that for the simpler case $l = e, \mu$ the bulk of the non-QED correction to the partial width can be absorbed into new $\tilde{\chi}_2^0 \tilde{l}_1 l$ couplings, which are sensitive to the spectrum of sfermions. In the case of τ final states, significant $\tilde{\tau}_L - \tilde{\tau}_R$ mixing as well as the τ Yukawa coupling have to be included in the analysis. We have not attempted to define such effective couplings and, perhaps, mixing angles here.

In this modified SPS1a scenario, the dilepton invariant mass distributions have a rather complicated shape, showing the contributions from Z exchange near the upper endpoints of the distributions. In this case the shape of these distributions is affected not only by real photon emission, which again leads to significant negative corrections for large $M_{l^+l^-}$, but also by virtual corrections, which can e.g. differ for Z and slepton exchange diagrams. In this case the shape of the distribution away from the endpoint also carries information about slepton masses and neutralino mixing angles. Fitting tree-level distributions to real data might therefore give wrong results for these physical parameters. In this context a careful analysis of collinear radiation is also important, since differences in the energy measurements of electrons and muons could lead to spurious differences of fitted selectron and smuon masses. Here the collinear-photon radiations for electrons and muons are treated as discussed beforehand. One finds that the one-loop shapes of the $M_{e^+e^-}$ and $M_{\mu^+\mu^-}$ distributions are different, though the selectrons and smuons have equal masses in our calculations.

We conclude that higher-order corrections to leptonic $\tilde{\chi}_2^0$ decays can exceed the 10% level both in integrated partial widths and branching ratios, and in the shape of the dilepton invariant mass distribution. Attempts to absorb much of the large virtual corrections into effective running couplings might be rewarding. An accurate understanding of $\tilde{\chi}_2^0$ decays is of considerable importance, since this is one of the lightest visible particles that can be produced directly at future e^+e^- colliders, and plays a prominent role in the analysis of cascade decays of gluinos and squarks at the LHC.

Acknowledgements

We would like to thank T. Fritzsche, T. Hahn, and H. Rzehak for helpful discussions, as well as A. Bredenstein and M. Roth for help with calculating the hard photon bremsstrahlung contribution. MD thanks the School of Physics at KIAS, Seoul, as well as the theory group at the university of Hawaii for hospitality.

Appendix

A Parameters

For the numerical evaluation, the following values of the SM parameters are used:

$$\begin{aligned} m_e &= 0.510999\text{MeV}, & m_\mu &= 105.6584\text{MeV}, & m_\tau &= 1.777\text{GeV}, \\ m_u &= 53.8\text{MeV}, & m_c &= 1.5\text{GeV}, & m_t &= 175\text{GeV}, \\ m_d &= 53.8\text{MeV}, & m_s &= 150\text{MeV}, & m_b &= 4.7\text{GeV}, \\ m_W &= 80.45\text{GeV}, & m_Z &= 91.1875\text{GeV}, \\ \alpha(0) &= 1/137.0359895, & G_\mu &= 1.1663910 \times 10^{-5}\text{GeV}^{-2}. \end{aligned}$$

The on-shell renormalization scheme requires $\alpha = \alpha(0)$ for one-loop calculations. For the tree level expressions we instead use the effective coupling for the overall normalization,

$$\alpha_{G_\mu} = \frac{\sqrt{2}G_\mu M_W^2 s_W^2}{\pi}. \quad (48)$$

We saw in Sec. 5 that this choice leads to good perturbative stability of the total $\tilde{\chi}_2^0$ decay width.

References

- [1] See e.g. M. Drees, R.M. Godbole and P. Roy, *Sparticles* (World Scientific, Singapore, 2004).
- [2] ATLAS Collab., *ATLAS Detector and Physics Performance Technical Design Report*, CERN/LHCC/99-5 (1999).
- [3] *TESLA Technical Design Report*, DESY 2001-011 (2001), hep-ph/0106315.
- [4] The LHC/LC Study Group, hep-ph/0410364.
- [5] A. Djouadi, M. Drees and J.L. Kneur, *JHEP* **0108** (2001) 055, hep-ph/0107316.
- [6] B.C. Allanach et al., *Eur. Phys. J.* **C25** (2002) 113, hep-ph/0202233;
G. Weiglein, hep-ph/0301111.
- [7] H. Baer, C.-h. Chen, M. Drees, F. Paige and X. Tata, *Phys. Rev. Lett.* **79** (1997) 986, hep-ph/9704457, and *Phys. Rev.* **D58** (1998) 075008, hep-ph/9802441;
I. Iashvili and A. Kharchilava, *Nucl. Phys.* **B526** (1998) 153, hep-ph/9712393;
A. Djouadi, Y. Mambrini and M. Mühlleitner, *Eur. Phys. J.* **C20** (2001) 563, hep-ph/0104115.
- [8] M.M. Nojiri and Y. Yamada, *Phys. Rev.* **D60** (1999) 015006, hep-ph/9902201.
- [9] W. Hollik, E. Kraus and D. Stöckinger, *Eur. Phys. J.* **C23** (2002) 735, hep-ph/0007134;
W. Hollik, E. Kraus, M. Roth, C. Rupp, K. Sibold and D. Stöckinger, *Nucl. Phys.* **B639** (2002) 3, hep-ph/0204350.
- [10] H. Eberl, M. Kincel, W. Majerotto and Y. Yamada, *Phys. Rev.* **D64** 115013 (2001) 115013, hep-ph/0104109;
W. Öller, H. Eberl, W. Majerotto and C. Weber, *Eur. Phys. J.* **C29** (2002) 563, hep-ph/0304006;
A. Arhrib and W. Hollik, *JHEP* **0404** (2004) 073, hep-ph/0311149;
K. Kovarik, C. Weber, H. Eberl and W. Majerotto, *Phys. Lett.* **B591** (2004) 242, hep-ph/0401092; *Phys. Rev.* **D72** (2005) 053010, hep-ph/0506021.
- [11] J. Guasch, W. Hollik and J. Solà, *JHEP* **10** (2002) 040, hep-ph/0207364.
- [12] T. Fritzsche and W. Hollik, *Eur. Phys. J.* **C24** (2002) 619, hep-ph/0203159.
- [13] W. Hollik and H. Rzehak, *Eur. Phys. J.* **C32** (2003) 127, hep-ph/0305328.
- [14] M. Frank, S. Heinemeyer, W. Hollik and G. Weiglein, hep-ph/0212037.
- [15] P. Chankowski, S. Pokorski and J. Rosiek, *Nucl. Phys.* **B423** (1994) 437;
A. Dabelstein, *Z. Phys.* **C67** (1995) 495.

- [16] A.B. Lahanas, K. Tamvakis and N.D. Tracas, *Phys. Lett.* **B324** (1994) 387, hep-ph/9312251;
D. Pierce and A. Papadopoulos, *Phys. Rev.* **D50** (1994) 565, hep-ph/9312248, and *Nucl. Phys.* **B430** (1994) 278, hep-ph/9403240.
- [17] G.F. Giudice and A. Pomarol, *Phys.Lett.* **B372** (1996) 253, hep-ph/9512337;
M. Drees, M.M. Nojiri, D.P. Roy and Y. Yamada, *Phys. Rev.* **D56** (1997) 276, Erratum-ibid. **D64** (2001) 039901, hep-ph/9701219.
- [18] Y. Yamada, *Phys.Rev.* **D54** (1996) 1150, hep-ph/9602279.
- [19] A. Freitas and D. Stöckinger, *Phys. Rev.* **D66** (2002) 095014, hep-ph/0205281.
- [20] M. Frank, S. Heinemeyer, W. Hollik and G. Weiglein, hep-ph/0202166.
- [21] A. Denner, *Fortschr. Phys.* **41** (1993) 307.
- [22] A. Sirlin, *Phys. Rev.* **D22** (1980) 971.
- [23] R. G. Stuart, *Phys. Lett.* **B272** (1991) 353;
D. Wackerroth and W. Hollik, *Phys. Rev.* **D55** (1997) 6788, hep-ph/9606398.
- [24] T. Hahn, *Comput. Phys. Commun.* **140** (2001) 418, hep-ph/0012260;
T. Hahn and C. Schappacher, *Comput. Phys. Commun.* **143** (2002) 54, hep-ph/0105349.
- [25] T. Hahn, *Nucl. Phys. Proc. Suppl.* **89** (2000) 231, hep-ph/0005029; *ibid.* **135** (2004) 333, hep-ph/0406288; hep-ph/0408247.
- [26] G. 't Hooft and M. Veltman, *Nucl. Phys.* **B153** (1979) 365.
- [27] W. Beenakker and A. Denner, *Nucl. Phys.* **B338** (1990) 349;
A. Denner, U. Nierste and R. Scharf, *Nucl. Phys.* **B367** (1991) 637.
- [28] A. Denner, S. Dittmaier, M. Roth and D. Wackerroth, *Nucl.Phys.* **B587** (2000) 67, hep-ph/0006307.
- [29] A. Bredenstein, S. Dittmaier, M. Roth, *Eur. Phys. J.* **C44** (2005) 27, hep-ph/0506005.
- [30] T. Kinoshita, *J. Math. Phys.* **3** (1962) 650; T.D. Lee and M. Nauenberg, *Phys. Rev.* **133** (1964) B1549.
- [31] F.A. Berends, R. Kleiss and R. Pittau, *Nucl. Phys.* **B424** (1994) 308, and *Comput. Phys. Commun.* **85** (1995) 437;
M. Roth, Ph.D thesis, hep-ph/0008033.
- [32] J.A. Aguilar-Saavedra et al., *Eur. Phys. J.* **C46** (2006) 43, hep-ph/0511344.

- [33] I. Hinchliffe, F.E. Paige, M.D. Shapiro, J. Soderqvist and W. Yao, *Phys. Rev.* **D55** (1997) 5520, hep-ph/9610544;
H. Bachacou, I. Hinchliffe and F.E. Paige, *Phys. Rev.* **D62** (2000) 015009, hep-ph/9907518;
M. Drees et al., *Phys. Rev.* **D63** (2001) 035008, hep-ph/0007202.
- [34] P.H. Chankowski, *Phys. Rev.* **D41** (1990) 2877;
K. Hikasa and Y. Nakamura, *Z. Phys.* **C70** (1996) 139, Erratum-ibid. **C71** (1996) 356, hep-ph/9501382;
H.-C. Cheng, J.L. Feng and N. Polonsky, *Phys. Rev.* **D56** (1997) 6875, hep-ph/9706438;
E. Katz, L. Randall and S.-f. Su, *Nucl. Phys.* **B536** (1998) 3, hep-ph/9801416;
S. Kiyoura, M.M. Nojiri, D.M. Pierce and Y. Yamada, *Phys. Rev.* **D58** (1998) 075002, hep-ph/9803210.
- [35] A. Birkedal, R.C. Group and K. Matchev, hep-ph/0507002.